Topographic Upwelling off Southwest Nova Scotia

KIM T. TEE AND PETER C. SMITH

Physical and Chemical Science Branch, Department of Fisheries and Oceans, Bedford Institute of Oceanography, Dartmouth, Nova Scotia, Canada

DENIS LEFAIVRE

Institut Maurice-Lamontagne, Department of Fisheries and Oceans, Mont-Joli, Quebec, Canada

(Manuscript received 30 July 1991, in final form 8 October 1992)

ABSTRACT

The waters off Cape Sable in southwestern Nova Scotia have anomalously low temperatures and high nutrients during summer. Using a three-dimensional tidal model as well as field observations obtained between 1978 and 1985, a new mechanism is proposed to explain the origin of these anomalous properties. The numerical model predicts several areas of strong tidally induced residual upwelling and downwelling. On the submarine ridge off Cape Sable, upwelling occurs over the eastern flank and downwelling over the western flank. This upward vertical transport is very effective in supplying cold, saline, and nutrient-rich water from deep to shallow layers. The predicted upwelling and downwelling are induced by a tidal rectification process resulting from tidal currents flowing over complex bottom topography. Hence, the process is named "topographic upwelling and downwelling."

The upwelling (downwelling) is generated by the residual currents flowing from deep to shallow (shallow to deep) waters. This process is three-dimensional so that the water parcels advected onshore from deep to shallow zones in the upwelling regime may remain in the lower layer and be carried away from the upwelling region by a longshore coastal current. Thus, the upward transfer of cold and saline water in the three-dimensional topographic upwelling may not be as efficient as the classical upwelling associated with two-dimensional (on–off shore) circulation. However, efficient vertical transfer can be accomplished in conjunction with the topographic upwelling if the cross-isobath transport associated with the upwelling carries deep water to a shallow region where there is strong vertical mixing. This combination of topographic upwelling and strong tidal mixing provides the mechanism for producing the observed cold water anomaly off Cape Sable. Topographic upwelling occurs on the eastern side of the cape, and strong tidal mixing produces a well-mixed area off the cape. These processes are verified by hydrographic, current meter, and Lagrangian drift data collected in the surrounding area. The mechanism is expected to be important in other coastal regions where strong tidal currents and large variations of bottom topography are found.

1. Introduction

The shelf waters off southwest Nova Scotia are among the most productive waters on the east coast of North America. They support major fisheries for lobster, groundfish, shellfish, and herring, and the largest concentration of nonbreeding surface-feeding seabirds in the northwest Atlantic (Kohler 1968). An important factor contributing to this productivity is a local upwelling characterized by low temperatures and high nutrients in the surface layer during summer (Bailey et al. 1954; Fournier et al. 1977; Smith 1983). The source of the upwelling water and the mechanisms forcing the upwelling are the subject of this study.

Using seabed drifter returns, Lauzier (1967) found a large-scale shoreward bottom current of approximately 0.02 m s^{-1} off southwest Nova Scotia. He suggested that the shoreward bottom drift was associated with an offshore surface drift, resulting in the upwelling along the coast. Garrett and Loucks (1976) proposed that the upwelling was driven by centrifugal forces associated with the strong tidal currents along the convex coastline near Cape Sable (Fig. 1). As the tide ebbs and floods along the coastline, the centripetal acceleration is balanced by a setdown of the sea surface at the coast. As the tidal currents reduce toward the bottom, the offshore pressure gradient drives an onshore flow in the bottom boundary layer, resulting in an upwelling near the coast. The magnitude of this "centrifugal upwelling" is 0.02 m s^{-1} off Cape Sable, about the same as the observed values obtained from the seabed drifter study. However, this simple model did not include longshore currents induced by the centrifugal force.

By including the depth-averaged Coriolis force on these currents, Smith (1983) estimated that the onshore bottom current was only 0.005 m s^{-1}, considerably

Corresponding author address: Dr. Kim T. Tee, Physical and Chemical Science Branch, Department of Fisheries and Oceans, Bedford Institute of Oceanography, P.O. Box 1006, Dartmouth, NS, B2Y 4A2, Canada.

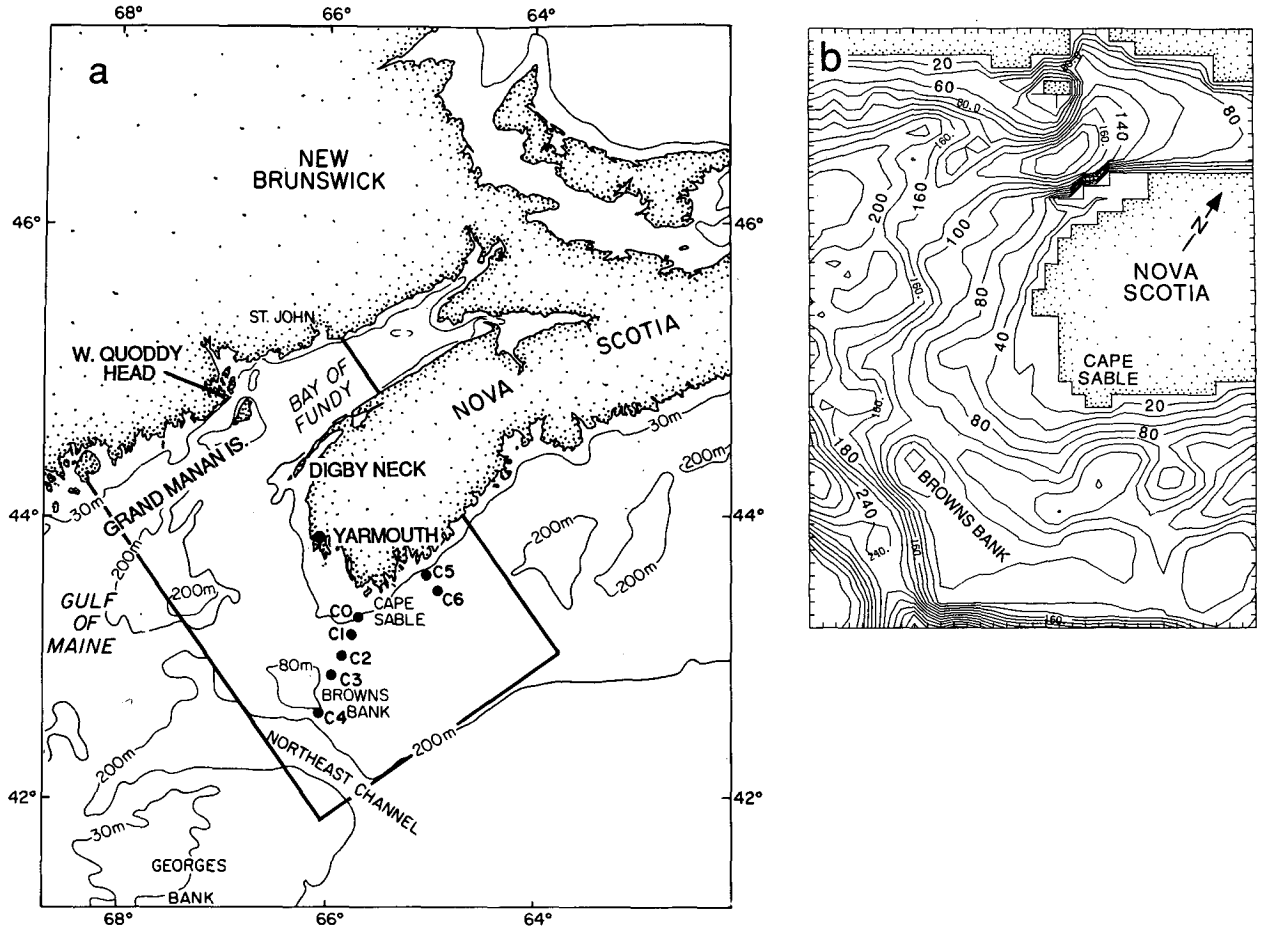

FIG. 1. (a) Location map for the Bay of Fundy and Gulf of Maine. The modeled area is enclosed by solid lines. (b) The topography of the modeled area. The distance between two tick marks on the boundaries in (b) is the grid spacing (7.047 km).

smaller than the observed values. He then suggested from results of a linear diagnostic model that the driving force for Cape Sable upwelling was the longshore density variations maintained by tidal mixing. However, the model flow in summer, driven primarily by the density variations, fails to reproduce the observed current (predicted eastward density flow as opposed to observed weak westward flow).

In fact, the suggested structure of simple upwelling off southwest Nova Scotia as the result of onshore bottom current and offshore surface current (Lauzier 1967; Garrett and Loucks 1976; Smith 1983) is not supported by the surface drifter data collected by Bumpus and Lauzier (1965), which showed that the surface currents near Cape Sable were onshore, in contradiction to the offshore currents required for upwelling. Although the wind is highly variable, the multiyear (1948–1962) collection of these drifter data may average out some of the variability. Also, the majority of the bottles had dry sand ballast to keep them upright near the surface and thus minimize the influence by direct wind forcing. More accurate measurements of the surface drift using satellite-tracked drogues (section 4f) also show the absence of this simple upwelling process. Hence, it appears that the cause of low temperatures and high nutrients near the sea surface off Cape Sable has not been explained satisfactorily.

In this study, a mechanism is proposed to describe consistently the upwelling and low temperature features near Cape Sable. Numerical simulations and field observations were used in the study. It will be shown that the upwelling process, named "topographic upwelling," is induced by three-dimensional rectification associated with tidal current flowing over complex bottom topography, and differs from a classical two-dimensional upwelling (onshore bottom current associated with offshore surface current) induced by wind, centrifugal, or density forcing.

The specific objectives of this paper are 1) to show the existence of the topographic upwelling off southwest Nova Scotia using both model simulations and field observations and 2) to describe a process (combined actions of topographic upwelling and tidal mixing) producing the cold water anomaly off Cape Sable. The

study is important scientifically because it presents a new dynamical mechanism to modify surface layer properties in shallow coastal waters that might also be expected to occur in other coastal areas where strong tidal currents flow over complex bottom topography, such as submarine banks. In addition, this process is important practically because it supplies nutrients from deep to surface layers in support of the high levels of biological productivity of the area. (For further details, see section 4b.)

The dynamics associated with the topographic upwelling process involve complex rectification arising from nonlinear interaction between tidal current and bottom topography. An example of the dynamics for an idealized (circular) submarine bank, which involve ten different forcing terms, is given by Tee (1993). A full understanding of the dynamics of topographic upwelling off Cape Sable, which involves complex structures of bottom topography, requires careful and extensive analysis. The needed analysis is beyond the scope of the present work but will be the subject of a future study.

The model-simulated upwelling and downwelling off southwest Nova Scotia are presented in section 2. A new mechanism to produce the cold water anomaly in shallow water is described in section 3. Verification of the model upwelling near Cape Sable from field observations, which include current meter measurements, hydrographic surveys, and Lagrangian drifter measurements, is carried out in section 4.

2. Model results

A simple method of calculating the three-dimensional tidal and residual currents has been developed (Tee 1979, 1980, 1987) and applied to the area southwest of Nova Scotia (Tee et al. 1987, 1988; Tee and Lefaivre 1990). In these previous studies, the model results were used mainly to examine the horizontal component of tidal and residual currents and to develop an accurate method for estimating the tidally induced residual current from current meter data. Here, we use the same model as well as field observations to show 1) the existence of the topographic upwelling and downwelling off southwest Nova Scotia and 2) the generation of a cold water anomaly there by the combined actions of topographic upwelling and tidal mixing.

The model domain (Fig. 1, enclosed by solid lines) has 41 levels in the vertical and 36×47 grid points in the horizontal. The horizontal grid spacing is uniformly 7.05 km, whereas the vertical spacing increases rapidly from the bottom as k^4 in the bottom boundary layer and as k^2 above that, where k is the number of vertical grid points measured from the bottom.

Only the M_2 tidal forcing is included in this model. It has been known that the large tidal range in the Gulf of Maine and Bay of Fundy system is due to the near resonance of the M_2 tide in the system. This large tidal range is simulated by Greenberg (1983) using a 2D large-scale depth-averaged model for the whole system. For the limited-area tidal model used here, the resonant characteristic of M_2 tidal oscillation is included simply by setting the tidal elevations at the open boundaries in the Gulf of Maine and Bay of Fundy (Fig. 1a) to those in Greenberg's model.

Figure 2 shows the depth-averaged residual currents (U_2) in the Cape Sable area. As indicated by Tee et al. (1987, 1988) and Greenberg (1983), the computed residual currents near the entrance to the Bay of Fundy (near Grant Manan Island, Fig. 1) are erratic. These irregular residual flows are due to resolution problems and not to the open boundary condition in our limited-area model. This conclusion is based on the fact that similar irregularities also occurred in two other large-scale depth-averaged tidal models (Greenberg 1983; Isaji and Spaulding 1984) that have similar horizontal grid spacing but that include the whole Gulf of Maine and Bay of Fundy system. By performing a series of numerical experiments, it was found that these irregular currents were limited only to the entrance of the Bay and did not significantly affect the residual circulation in the Cape Sable area, because the circulation there is induced locally by topographic variations (Tee and Lefaivre 1990). Furthermore, a recent simulation of the residual current using a fine-grid 3D tidal model (3.5 km grid; to be published) has shown that the overall residual circulation near Cape Sable is basically the same as in the coarse-grid model. Also, the model tidal and residual currents, and tidal elevation, compare well with observations near Cape Sable (Tee et al. 1987, 1988) and agree with the depth-averaged results of the large-scale models (Greenberg 1983; Isaji and Spaulding 1984). Thus, the residual currents near Cape Sable are reliable. In the following, only these currents in the southeastern part of the model's domain (Fig. 1) are discussed.

In the offshore area, the horizontal diffusion of momentum is neglected. This approximation has been included in many tidal models (e.g., Nihoul and Ronday 1975; Flather and Heaps 1975; Davies 1980; and Greenberg 1983). One reason for making this approximation is that the horizontal diffusion coefficient is very uncertain. Another is that, by taking reasonable values of the coefficient, the diffusion term is found to be generally much smaller than the bottom friction term in these coastal basins. As an example, we consider the area around Cape Sable where the cold water anomaly occurs. By taking the values of the horizontal diffusion coefficient (A_h) to be $\sim 10^2$ m^2 s^{-1} (Holloway 1981; Zimmerman 1986), the horizontal length scale (L) to be $\sim$20 km (about three grid spacings, Fig. 2), the depth scale (D) to be $\sim$40 m, the bottom friction coefficient (C_D) to be $\sim$0.0021, and the tidal current (U_m) to be ~ 1 m s^{-1}, we estimate the ratio of the horizontal diffusion term to bottom friction term

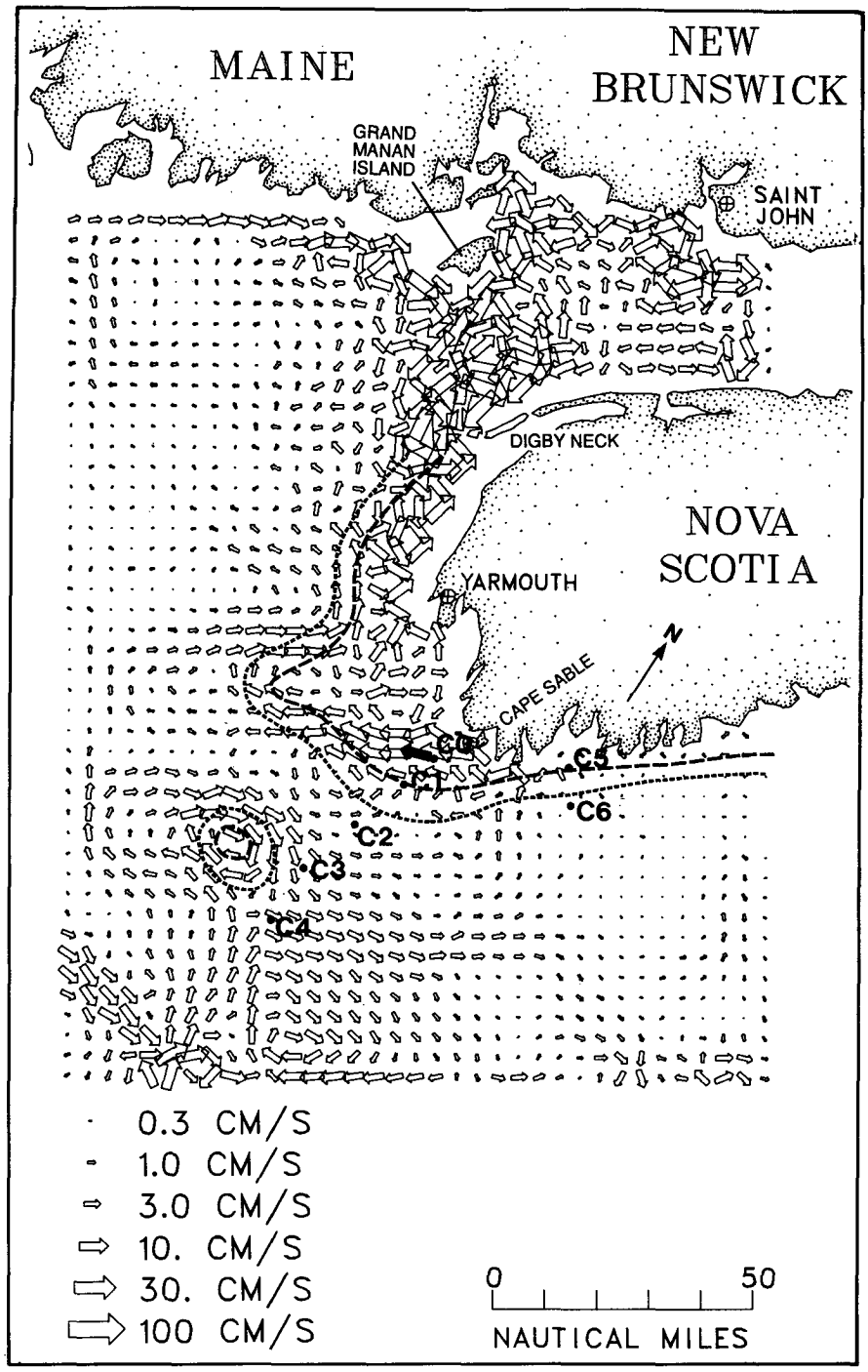

FIG. 2. The computed depth-averaged residual currents induced by the M_2 tide. The 60-m and 80-m isobaths off Cape Sable and on Browns Bank are indicated by dashed and dotted curves. The current meter stations (C0 to C6) are indicated by solid circles. The observed tidally induced residual current at station C0 (Tee et al. 1988) is indicated by a solid arrow.

$[(A_h/L^2)/(C_DU_m/D)]$ to be ~0.005, about two to three orders of magnitude smaller than one. Some numerical models include the horizontal diffusion to damp out the numerical subgrid oscillations [e.g., coarse-grid model of Greenberg (1983)].

Stratification in the water column may affect the

vertical mixing coefficient. However, this effect on the topographic rectified residual circulation has been found to be small (Tee 1985). Residual currents induced directly by wind and density forcing may be significant. The contribution of these currents to the upwelling feature off Cape Sable remains to be investigated. Here, we show that the upwelling induced solely by the tidal forcing can consistently explain the occurrence of the cold water anomaly off the cape.

a. The vertical velocity

Using the horizontal residual currents, the vertical residual currents can be computed from the continuity equation (Tee 1993). The spatial distribution of Eulerian upwelling and downwelling (w_2) near Cape Sable (Fig. 3) indicates that upwelling (solid curves) occurs mainly on the eastern side, and downwelling (dashed curves) on the western side. West of the downwelling area (south of Yarmouth), there is also a small upwelling area. On Browns Bank, upwelling occurs on the northwestern and southeastern sides, and downwelling on the northeastern and southwestern sides. The upwelling and downwelling on the western side are significantly greater than those on the eastern side. Near the southern corner of the open boundary, upwelling occurs on the eastern side of Georges Bank and along the eastern slope of Northeast Channel,

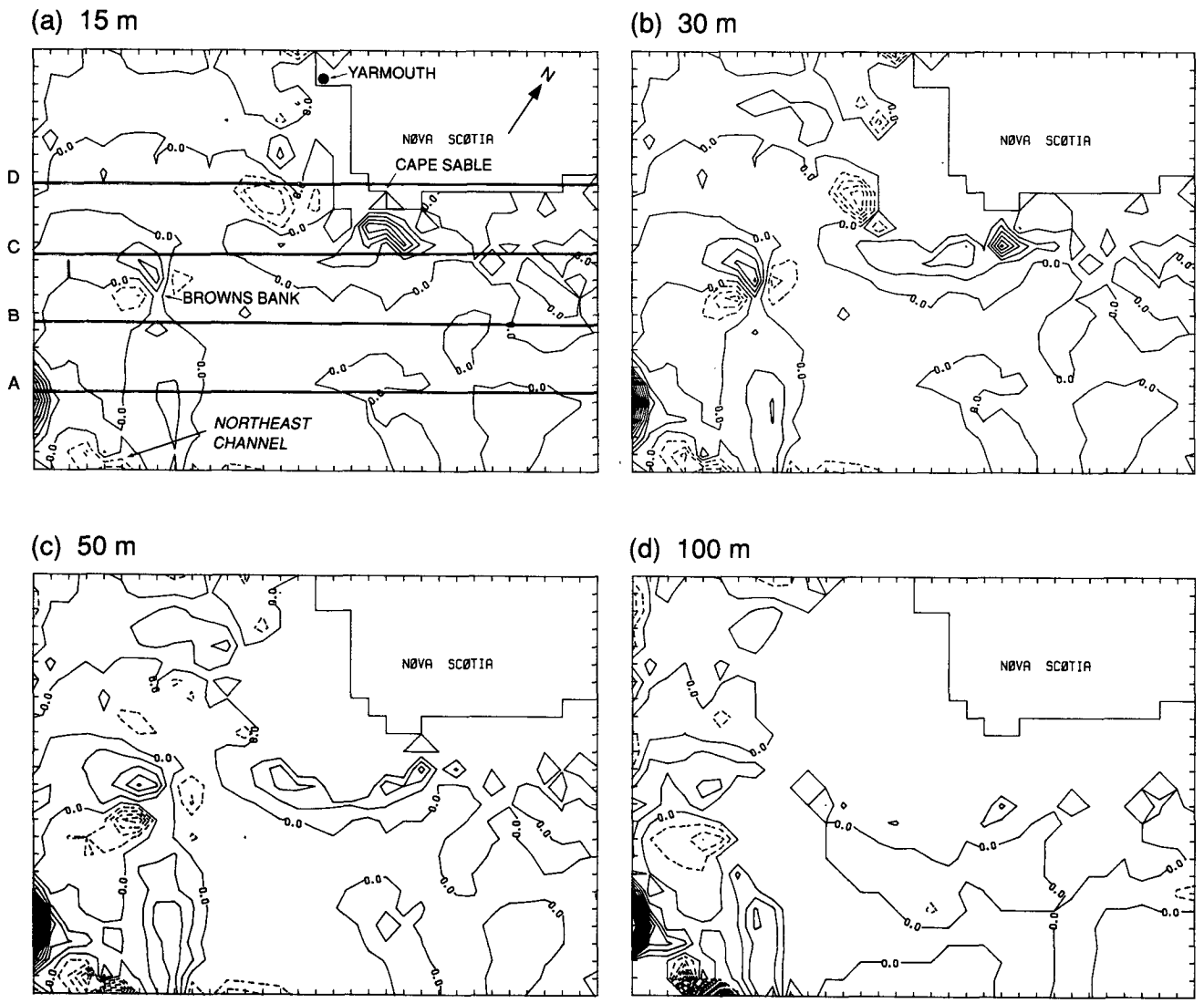

FIG. 3. The Eulerian component of the vertical residual current, w_2 (10^{-5} m s^{-1}), at (a) 15 m, (b) 30 m, (c) 50 m, and (d) 100 m. Positive w_2 are indicated by solid curves, and negative w_2 by dashed curves. The contour interval is 2×10^{-5} m s^{-1}. The distance between two tick marks on the boundaries is 7.047 km. The four horizontal lines (A, B, C and D) in (a) indicate the sections where the vertical structure of w_2 is shown in Fig. 4.

and downwelling occurs in the central portion of the channel.

By examining the vertical velocity in the water column (compare Fig. 3a to Figs. 3b–d), we can see that the upwelling and downwelling extend throughout the water column. For example, the upwelling on the eastern side of Cape Sable and the northwestern side of Browns Bank extends from 15 to 100 m. By examining in Fig. 4 the variation of w_2 along the sections A, B, C, and D (Fig. 3a), we see that the vertical velocity generally increases from the surface to a maximum value in the lower half of the water column.

The Lagrangian vertical velocity (w_{2L}) can be computed from the convergence and divergence of the horizontal Lagrangian residual currents. Figure 5 shows the currents at 15, 30, 50, and 100 m. By comparing Figs. 3 and 5, we can see that the spatial structures of Eulerian and Lagrangian vertical velocities are generally the same. However, the magnitudes of upwelling and downwelling can be significantly different. The magnitudes of the Lagrangian vertical velocities are greater than the Eulerian components in the upwelling areas on the eastern side of Cape Sable and the southeastern side of Browns Bank and in the downwelling areas on the northeastern side of Browns Bank. On the other hand, Eulerian exceed Lagrangian vertical velocities in the upwelling areas south of Yarmouth, on the northwestern side of Browns Bank, the eastern side of Georges Bank, and the eastern slope along the Northeast Channel and in the downwelling areas west

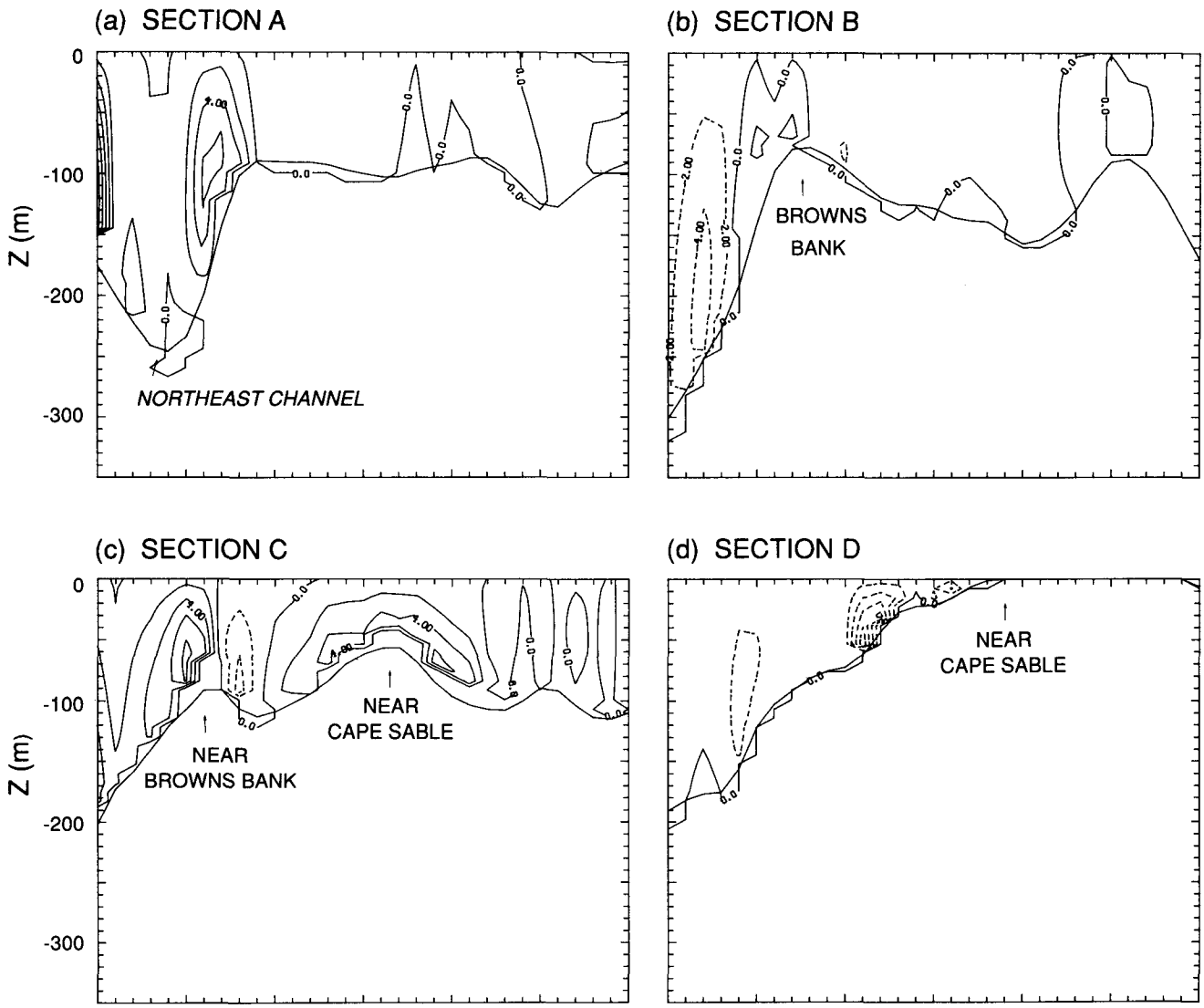

FIG. 4. The structure of w_2 (10^{-5} m s^{-1}) along sections A, B, C, and D shown in Fig. 3a. The distance between two tick marks on the x axis is 7.047 km. See Fig. 3 caption for further details.

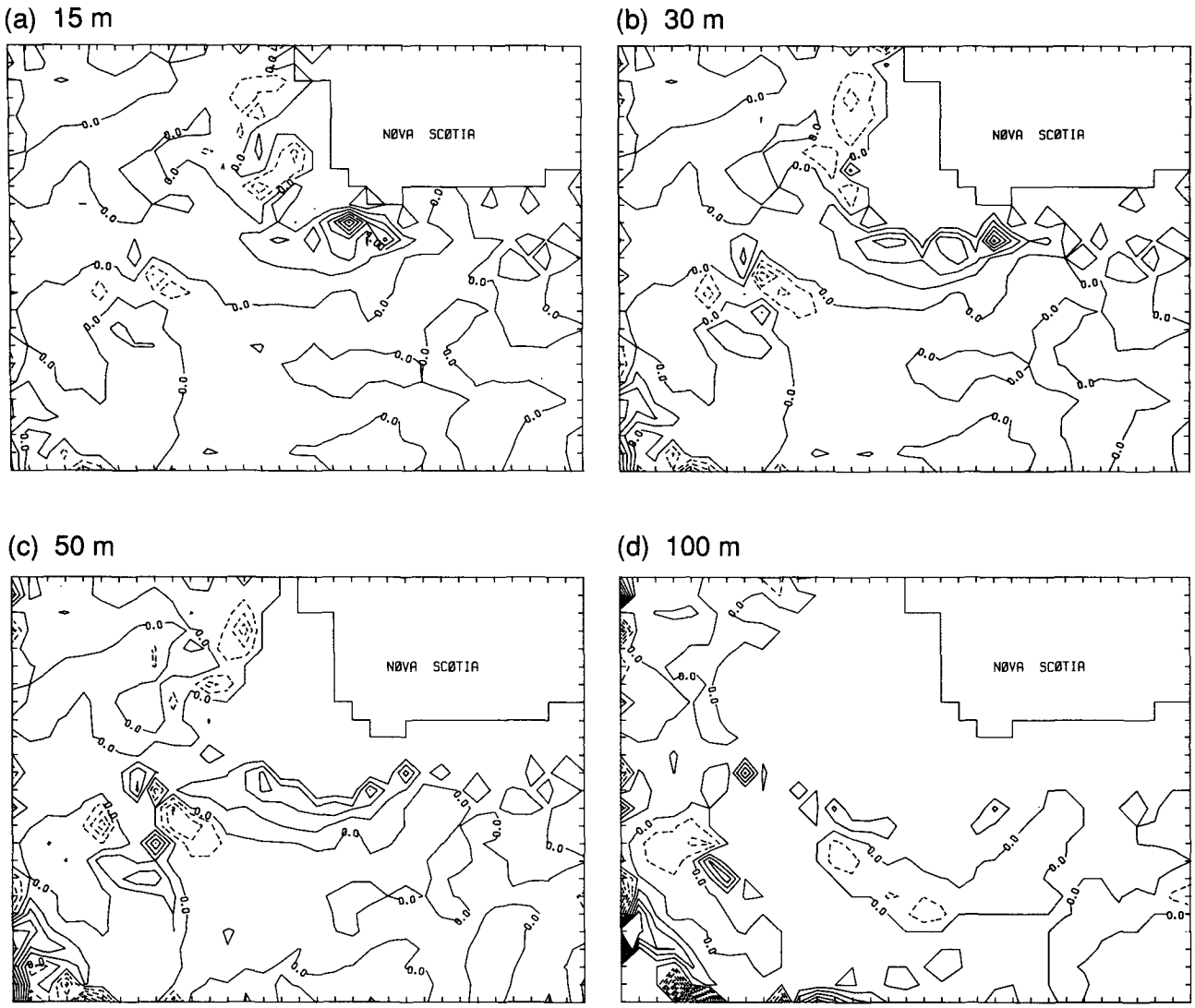

FIG. 5. Lagrangian component of the vertical residual current, w_{2L} (10^{-5} m s^{-1}). See Fig. 3 caption for further details.

of Cape Sable, on the southwestern side of Browns Bank, and in the central portion of the Northeast Channel. These complex variations between Eulerian and Lagrangian components of the vertical velocities are induced not only by the differences in the magnitude of the horizontal residual currents but also by the slight variations of their circulation patterns.

b. Topographic upwelling and downwelling

In coastal water, the upwelling (or downwelling) is frequently associated with a two-dimensional circulation that features onshore (offshore) flow in the lower portion of water column and offshore (onshore) flow in the upper portion. The depth-averaged cross-isobath flow is negligibly small in this two-dimensional case. Examples of such processes include 1) wind-driven upwelling (downwelling) in which offshore (onshore) Ekman transport in the surface layer is balanced by onshore (offshore) flow at depth and 2) the freshwater-induced estuarine circulation, which results in an upwelling near the head of an estuary. In a three-dimensional case, the upward or downward water motion generated by convergence or divergence of cross-isobath flows can be compensated by divergence or convergence of the alongisobath currents. Thus, the deep-water parcels that are advected shoreward in the upwelling regime can be moved away by the alongisobath current, and are not required to ascend all the way to the surface layer in order to feed an offshore return flow. The depth-averaged cross-isobath flow is significant in this case. The model circulation to the southwest

of Nova Scotia is an example of such a three-dimensional process.

The tidally induced residual currents in the Cape Sable area decrease weakly from surface to bottom (Tee et al. 1987; see also Fig. 12). The upwelling and downwelling are thus not associated with the two-layer circulation. They are induced by those residual currents that cross isobaths. A clear example is the upwelling east of Cape Sable where the residual currents are directed from deep to shallow water (Fig. 2). A strong westward jet is formed by the convergence of these cross-isobath currents. As the jet crosses isobaths from shallow to deep water on the western side of Cape Sable, downwelling is induced (Figs. 2 and 3). The magnitudes of the residual currents are reduced in the deeper water due to the deepening of the westward jet. Some of the deep-water parcels return to shallow water farther west and form the upwelling region south of Yarmouth. Similar processes can be found to form the upwelling and downwelling regions on Browns Bank and Northeast Channel.

The spatial structure of upwelling or downwelling induced by cross-isobath residual flow can be examined by the value of $-\mathbf{U}_2 \cdot \nabla D$, where $\mathbf{U}_2$ is the depth-averaged residual velocity and D is depth of the water column (see the Appendix). Upwelling (downwelling) is induced if the flow is directed from deep to shallow (shallow to deep) water such that $-\mathbf{U}_2 \cdot \nabla D$ is positive (negative). Comparing the spatial distribution of $-\mathbf{U}_2 \cdot \nabla D$ (Fig. 6) to vertical velocities (Fig. 3) confirms that the upwelling and downwelling areas correspond very well with the positive and negative values of $-\mathbf{U}_2 \cdot \nabla D$. An example is the upwelling area east of Cape Sable. Figure 7 shows that the computed depth-averaged vertical velocity (W_2) and $-\mathbf{U}_2 \cdot \nabla D$ are well

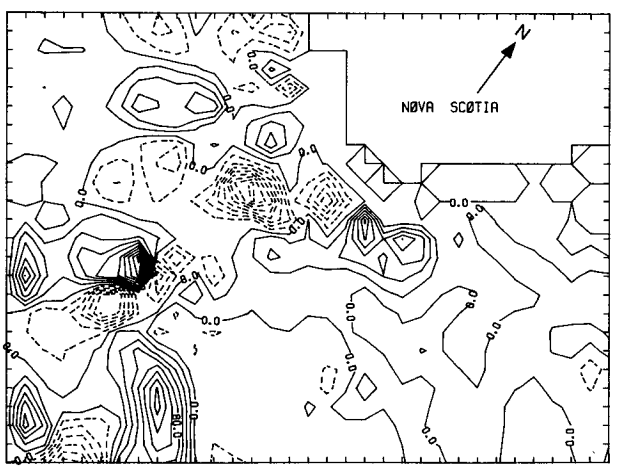

FIG. 6. The spatial distribution of $-\mathbf{U}_2 \cdot \nabla D$ in units of 10^{-5} m s^{-1}, which indicates the vertical velocity induced by the depth-averaged cross-isobath residual currents. The contour interval is 2×10^{-5} m s^{-1}. See Fig. 3 caption for further details.

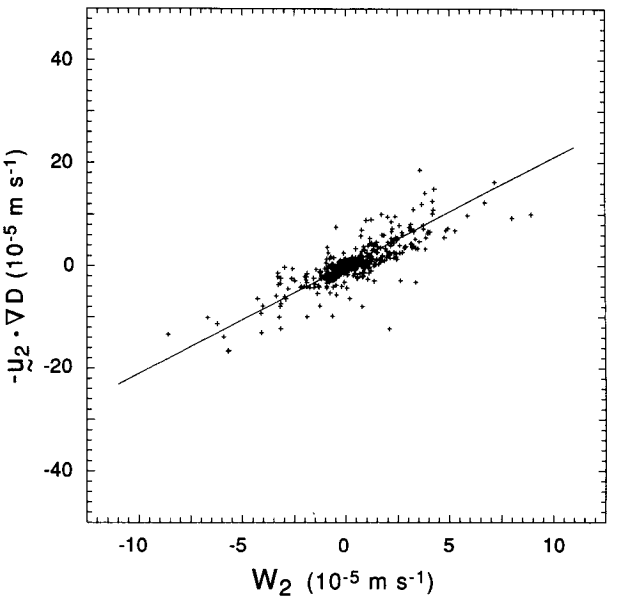

FIG. 7. The comparison between W_2 (depth-averaged w_2) and $-\mathbf{U}_2 \cdot \nabla D$. The value at each grid point is indicated by a plus sign. A least-squares fit of the data gives $-\mathbf{U}_2 \cdot \nabla D = -0.36 \times 10^{-6}$ m s^{-1} $+ 2.10 W_2$, which is shown by a solid line.

correlated (correlation coefficient = 0.85). A linear regression of all the data points gives

$$-\mathbf{U}_2 \cdot \nabla D = -0.36 \times 10^{-6} \text{ m s}^{-1} + 2.10 W_2. \quad (1)$$

The intercept value of -0.36×10^{-6} m s^{-1} is negligibly small compared to the computed W_2 in the major upwelling and downwelling areas. The slope of 2.10 between $-\mathbf{U}_2 \cdot \nabla D$ and W_2 is induced mainly by the variation of the vertical velocity in the water column. For uniform values of the tidally induced residual currents in the water column, which approximates the smooth profiles of the residual current southwest of Nova Scotia (Tee et al. 1987; also see Fig. 12), the vertical residual current (w_2) decreases linearly from $-\mathbf{U}_2 \cdot \nabla D$ near the bottom to about zero on the surface (Appendix). The depth-averaged value of w_2 is then approximately equal to half of $-\mathbf{U}_2 \cdot \nabla D$.

The modeled vertical circulation off southwest Nova Scotia is generated mainly by topographic effects since the horizontal residual currents (and thus the vertical velocity) have been found to be negligibly small if the depths in this region are made uniform (Tee and Lefaivre 1990). Because of this topographic effect, the upward and downward movement of water parcels by the residual currents are called "topographic upwelling and downwelling." The residual eddies induced by coastal headlands, such as those computed by Tee (1976, 1977) and Pingree and Maddock (1977), are found to exist only in the nearshore area within about 10 km from the Nova Scotian coastline. This is because

the coastal boundary effect in the weakly nonlinear case, such as that southwest of Nova Scotia, is limited near the coast [order of a tidal excursion ($\sim$10 km)].

The good correlation between the cross-isobath residual current and the topographic upwelling and downwelling is due to two particular characteristics of the topographic rectification process. The first is the existence of significant cross-isobath residual flow, and the second is the smooth variation of that residual flow with depth. As tides off southwest Nova Scotia, whose wavelength [O (100 km)] is much longer than the topographic length scale [O (10 km)], flow over uneven bathymetry, topographic rectification of the first-order tidal current produces strong forcing for the second-order residual current. This strong forcing can overcome vorticity constraints for flow along f/D contours and generate significant cross-isobath residual currents (Fig. 2; also see Tee 1992). Because the tidal currents vary weakly in most of the vertical water column except at the thin bottom logarithmic layer, the nonlinear tidal forcing and thus the second-order residual currents are only weakly sheared (Tee et al. 1987). Thus, the vertical structure of topographic upwelling and downwelling is part of the characteristics of the tidal rectification process.

The close correlation between the vertical residual current and the depth-averaged horizontal residual currents indicates that the computed topographic upwelling and downwelling are insensitive to the numerical scheme applied in this study. This may be deduced from the fact that similar depth-averaged tidal and residual circulations are produced by our model (Fig. 2) and two other large-scale 2D models [Fig. 10 of Greenberg (1983); Fig. 5 of Isaji and Spaulding (1984)], which have similar grid spacing (about 7 km) but different numerical schemes. For example, all the models show that the depth-averaged residual currents on the eastern side of Cape Sable are directed from deep to shallow waters (e.g., Fig. 2), which corresponds to the topographic upwelling in that area (Figs. 3 and 6).

The importance of the topographic upwelling on the eastern side of Cape Sable can be seen by comparing the upwelling with the wind-induced upwelling on a typical continental shelf. Taking the upwelling velocity to be 3–4 ($\times 10^{-5}$ m s^{-1}) and the width of upwelling zone to be 30 km (Fig. 3), the topographic upwelling transport per unit alongshore distance is about 1.0 m^2 s^{-1}. For an upwelling-favorable alongshore wind stress, τ_w, the vertical transport per unit alongshore distance is $\tau_w/\rho f$, where ρ is the density of water and f ($\sim 10^{-4}$ s^{-1}) is the Coriolis parameter. To produce a vertical transport equivalent to that of topographic upwelling ($\sim$1.0 m^2 s^{-1}), a fairly strong wind speed of $\sim$7 m s^{-1} is required. This wind speed is about three times the averaged upwelling wind speed on the Scotian Shelf in summer (about 2.4 m s^{-1}; Petrie et al. 1987; Lively 1984, 1985). The vertical transport per unit alongshore distance induced by topographic upwelling off Cape Sable is thus about nine times that induced by the wind stress over the Scotian Shelf in summer. However, the ratio for the total vertical transport by these two forcings may be comparable because the horizontal scale for the topographic upwelling is $\sim$50 km, and that for the Scotian Shelf is $\sim$500 km.

3. A mechanism to produce a cold water anomaly in shallow water

A mechanism to produce a cold water anomaly off Cape Sable is described in this section. To understand the physical process, we examine the effects of surface heat flux and topographic upwelling on the heat content and temperature of the water column.

For a Cartesian system with horizontal coordinate x and y and vertical coordinate z, measured vertically upward from the mean sea level ($z = 0$), the equation describing the long-term variation of temperature (T) can be written as

$$\frac{\partial T}{\partial t} + \mathbf{u}_2 \cdot \nabla T + w_2 \frac{\partial T}{\partial z} = \frac{\partial}{\partial z} N \frac{\partial T}{\partial z}, \qquad (2)$$

where $\mathbf{u}_2$ and w_2 are the horizontal and vertical residual currents, t is time, N is the vertical eddy diffusivity, and ∇ is the horizontal gradient operator. The horizontal diffusion is neglected here because the time scale of the vertical diffusion in coastal water is generally much shorter than that of the horizontal diffusion (section 2; also see Loder et al. 1988). By using the continuity equation of the residual current (A1), Eq. (2) can be rewritten as

$$\frac{\partial T}{\partial t} + \nabla \cdot \mathbf{u}_2 T + \frac{\partial}{\partial z} w_2 T = \frac{\partial}{\partial z} N \frac{\partial T}{\partial z}. \qquad (3)$$

By using the boundary conditions of $w_2 = 0$ (or $w_2 = -\mathbf{u}_{2b} \cdot \nabla D$, where $\mathbf{u}_{2b}$ is the bottom residual current) and $\partial T/\partial z = 0$ at the bottom ($z = -D$), and $w_{20} = \nabla \cdot \overline{\mathbf{u}_{10}\zeta_1}$ (Tee 1993) and $\rho c_p \partial T/\partial z = Q$ at the surface ($z = 0$), where D is water depth, ρ is density of water, c_p is the specific heat, Q is the surface heat flux, u_{10} is the tidal current at the surface, w_{20} is the value of w_2 at surface, ζ_1 is the tidal elevation, and the overbar denotes the time average over the tidal cycle, the depth-averaged equation of (3) is

$$\frac{\partial \tilde{T}}{\partial t} + \frac{1}{D} \nabla \cdot D\langle \mathbf{u}_2 T \rangle + \frac{T_0}{D} \nabla \cdot \overline{\mathbf{u}_{10}\zeta_1} = \frac{Q}{\rho c_p D}, \qquad (4)$$

where $\tilde{T}$ is the depth-averaged temperature, T_0 is the surface temperature, and

$$\langle \mathbf{u}_2 T \rangle = \frac{1}{D} \int_{-D}^{0} \mathbf{u}_2 T dz \qquad (5)$$

is the depth average of ($\mathbf{u}_2 T$). Because the tidally in-

duced residual currents in the Cape Sable area are only weakly sheared over the water column, $\langle u_2 T \rangle$ can be approximated by $U_2 \tilde{T}$ (section 4a), where U_2 is the depth-averaged u_2. Using this approximation, (4) can be rewritten as

$$\frac{\partial \tilde{T}}{\partial t} + \frac{1}{D} \nabla \cdot D\mathbf{U}_2 \tilde{T} + \frac{T_0}{D} \nabla \cdot \overline{\mathbf{u}_{10} \zeta_1} = \frac{Q}{\rho c_p D}. \quad (6)$$

From the continuity equation of the depth-averaged residual current (A4), Eq. (6) can be reduced to

$$\frac{\partial \tilde{T}}{\partial t} + \mathbf{U}_2 \cdot \nabla \tilde{T} + \frac{(\tilde{T} - T_0)}{D} \nabla \cdot \overline{\mathbf{u}_{10} \zeta_1} = \frac{Q}{\rho c_p D}. \quad (7)$$

The third term on the left-hand side of (7) is due to the advection of temperature by the vertical residual current at the surface. This term can be neglected because the vertical residual current is small at the surface (Fig. 4, also see the Appendix). Equation (7) can then be written as

$$\frac{d\tilde{T}}{dt} \approx \frac{Q}{\rho c_p D}, \quad (8)$$

where $d/dt = (\partial/\partial t + \mathbf{U}_2 \cdot \nabla)$ is the total derivative, that is, following a water column. Similar results can be obtained for the depth-averaged salinity ($\tilde{S}$) and nitrate concentration ($\tilde{C}$):

$$\frac{d}{dt}(\tilde{S}, \tilde{C}) = 0. \quad (9)$$

Despite the fact that the time scales for nitrate uptake by phytoplankton under optimum growth conditions are of order one day to one week (G. Harrison, personal communication), we have considered nitrate to be a conservative property because 1) the intense tidal mixing off Cape Sable limits phytoplankton growth by reducing the average light input to a given water parcel (Fournier et al. 1984) and 2) the horizontal advection time scale for a well-mixed water parcel near the frontal zone (e.g., station 10) is smaller than that associated with uptake. The consistency of these assumptions will be tested in section 4d.

By neglecting the small variation of density, (8) can be written in terms of the heat content per unit surface area ($h = \rho c_p D \tilde{T}$),

$$\frac{dh}{dt} - \frac{h}{D} \mathbf{U}_2 \cdot \nabla D = Q. \quad (10)$$

For a given heat flux (Q), Eq. (8) indicates that the depth-averaged temperature of a water column increases more slowly in a deeper region. Thus, a water column that remains in an offshore deep region during the heating season (spring and summer) is expected to have a lower depth-averaged temperature than one in an inshore shallow region. During advection from deep to shallow waters by the tidally induced residual current, water parcels are advected upward by topographic upwelling. The time scale of this upwelling process is short (in days, subsection 4c) so that the effect of surface heat flux on the water temperature is small. We can write the depth-averaged temperature in shallow [$\tilde{T}$(shallow)] and deep [$\tilde{T}$(deep)] regions approximately as

$$\tilde{T}_{n+1}(\text{shallow}) = \tilde{T}_n(\text{deep}) + \frac{Q}{\rho c_p D_A} \Delta t \quad (11)$$

and

$$\tilde{T}_{n+1}(\text{deep}) = \tilde{T}_n(\text{deep}) + \frac{Q}{\rho c_p D_p} \Delta t, \quad (12)$$

where the subscripts n and $n + 1$ denote the times when the cross-isobath advection starts and ends; Δt is the time interval of the advection; D_A is the averaged depth between deep and shallow regions; and D_p is the depth of the deep region. [Note that $\tilde{T}_n$(deep) is assumed to be more and less uniform spatially.] For the topographic upwelling area on the eastern side of Cape Sable, it will be shown in subsection 4c that the contribution of the surface heat flux over an advective time scale is small, and hence, the depth-averaged temperature is approximately conserved; that is,

$$\tilde{T}_{n+1}(\text{shallow}) \approx \tilde{T}_{n+1}(\text{deep}). \quad (13)$$

Thus, the depth-averaged temperature of the upwelled water in the shallow region is approximately equal to that in the deep region. Because the increase of water temperature by surface heat flux during the heating season is slower in the deeper region, the upwelled water is colder than the resident water in the shallow zone that has been affected by surface heat flux alone.

The conservation of depth-averaged temperature (13) in the topographic upwelling area results in the heat loss per unit area in the water column (10). The upwelling process reduces the column thickness (D) by ΔD, where $\Delta D = D(\text{deep}) - D(\text{shallow})$. The amount of heat loss per unit area resulting from the change of column thickness is $-h\Delta D/D$. The time required to move the water column from deep to shallow regions is $\Delta L/U_{2c}$, where ΔL is the distance between the two locations and $\mathbf{U}_{2c}$ is the cross-isobath residual current. The rate of heat loss per unit area is then equal to $(-h\Delta D/D)/(\Delta L/\mathbf{U}_{2c})$, which can be written as $(-h/D)\mathbf{U}_2 \cdot \nabla D$ [second term on the left-hand side of (10)].

Although the advection of water parcels from deep to shallow regions by the topographic upwelling can produce low depth-averaged temperature in the shallow water region, the existence of cold surface temperature in this region requires strong vertical mixing. This is because the topographic upwelling is a three-dimensional feature; the cold water in the lower layer, although it is upwelled from deep to shallow regions, can

remain mostly in the lower layer in the shallow region. The penetration of cold water from lower to upper layers will be efficient if the water parcels are mixed uniformly in the water column before they are advected away by coastal currents. In coastal waters the vertical penetration can be induced by strong tidal mixing. This combination of topographic upwelling and tidal mixing will be shown in the next section to be the mechanism that produces the cold surface water in the Cape Sable area.

4. Evidence of the topographic upwelling near Cape Sable

Because the topographic upwelling is part of the cold-water formation process in shallow water, we can demonstrate this upwelling by examining carefully the occurrence and distribution of the cold water anomaly. Section 4a describes the occurrence of this anomaly off Cape Sable. The possibility of producing the anomaly by the combined actions of topographic upwelling and tidal mixing is outlined in section 4b. The conservation of depth-averaged temperature during the topographic upwelling process, the key factor in formation of the cold water anomaly, is examined in section 4c. Evidence of the topographic upwelling off Cape Sable from detailed analyses of temperature, salinity, and nitrate concentration on various hydrographic sections is shown in section 4d. Further evidence of the upwelling from current meter and Lagrangian drifter data is discussed in sections 4e and 4f.

a. Low temperature around Cape Sable

As indicated in the Introduction, the waters around Cape Sable in summer are much colder than other areas in the Gulf of Maine with similar depths and currents. For example, the water temperature near Cape Sable in midsummer is ~7°C, much colder than the well-mixed water on the cap of Georges Bank (15°C; Flagg 1987). This low temperature was observed previously from short period measurements, such as hydrographic surveys and satellite images. Here, we examine these cold waters from long-term current meter measurements and a detailed hydrographic survey in 1979.

Between November 1978 and May 1985 a field program to investigate the circulation and physical properties off southwest Nova Scotia was carried out (Smith 1983, 1989a, 1989b). Off Cape Sable there were seven current meter stations (C0 to C6) with three to eight current meters per station (Fig. 8). The cold water anomaly around the cape can be investigated using long-term temperature measurements from two inshore current meter records at stations C0 and C1, the two stations nearest to the cape (Fig. 8). Station C0 is

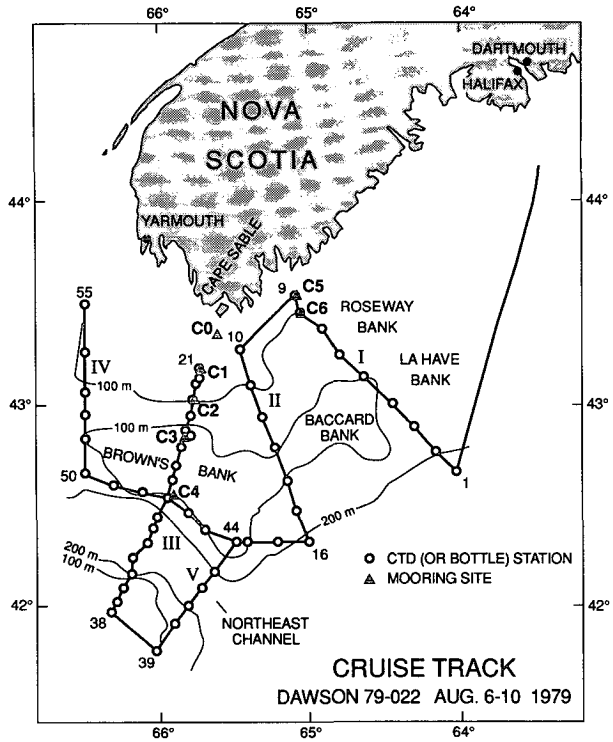

FIG. 8. The cruise track carried out between 6 and 10 August 1979. CTD stations (from 1 to 55) are indicated by open circles, and current meter stations (C0 to C6) by solid triangles.

located in well-mixed water, and station C1 is near the frontal region (between well-mixed and stratified waters) where temperature generally varies only slightly in the vertical. The water column for the other stations was stratified in summer. The temporal variations of temperature for the two stations were found to be very similar. Here, only the longer records for station C1 are discussed.

The temperature records at 16 m (solid) and 30 m (dashed) at station C1 in 1979 (Fig. 9) reveal that the temperature increases gradually from 4°C in early May to about 10°C in mid-September. During July and August, the temperature varies between 7° and 9°C. These low temperatures were also recorded at C1 in the subsequent three years. However, the low temperature regimes in these years were interrupted by short-period warm events (Lively 1984, 1985). The warm events, with maximum temperatures of 14°–17°C, lasted for 10–15 days in 1980 and 1981 and about 25 days in 1982 and were associated with low salinities. The events occurred three times in 1980 and one time each in both 1981 and 1982. An examination of wind forcing and the temperature, salinity, and velocity variations at various stations suggests that these events were related to a southwestward wind that produced downwelling and longshore currents in the downwind direction on the Scotian Shelf. The warm

and fresh water (in comparison to Cape Sable water) in the upper layer of the shelf, accumulated by onshore currents during the downwelling event, was advected by longshore currents to the Cape Sable area.

The hydrographic data were collected mostly in the early spring (March–May) and fall (October–November). The only summer (August) data were collected in 1979 and 1980. The 1980 summer cruise coincided with one of the warm events in the Cape Sable area, and is thus not applicable for the present studies of the topographic upwelling. The 1979 summer data, collected between 6 and 10 August (between days 218 and 222), provides our only detailed description of normal summer oceanographic conditions in this area. We will use these data and the 1979 long-term temperature records (Fig. 9) to show the existence of the topographic upwelling on the eastern side of Cape Sable, and the production of the cold water anomaly off the cape by the combined actions of this upwelling and the tidal mixing.

Figure 8 shows the 1979 cruise track and the CTD and current meter stations. Surface temperature was also measured from a hull-mounted thermistor. Figure 10 shows the surface temperature derived from these two datasets. We can see that there is a pronounced cold water anomaly off Cape Sable, with recorded temperatures below 7°C. Such an anomaly near Cape Sable has been indicated by several previous studies (Bailey et al. 1954; Fournier et al. 1977; Garrett and Loucks 1976; and Smith 1983). The extent of this cold water west of Cape Sable cannot be drawn in Fig. 10 because of insufficient coverage of the hydrographic station data in this shallow water area (Fig. 8). However, surface temperature derived from satellite imagery clearly shows the occurrence of this anomaly locally around Cape Sable (Fig. 2 of Smith 1983). Extensive analysis of satellite images near southwest Nova Scotia for the year 1984 shows similar results (to be published).

b. Cold water anomaly induced by topographic upwelling and tidal mixing

A well-mixed water column in a shallow region can be induced by strong tidal mixing. Using hydrographic data from the Bay of Fundy and Gulf of Maine and

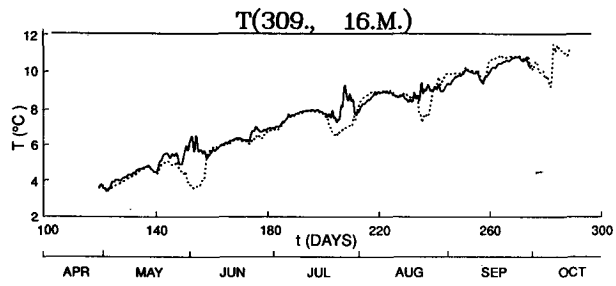

FIG. 9. Observed temperature variations in 1979 at 16 m (solid) and 30 m (dashed) at current meter station C1 (Fig. 8).

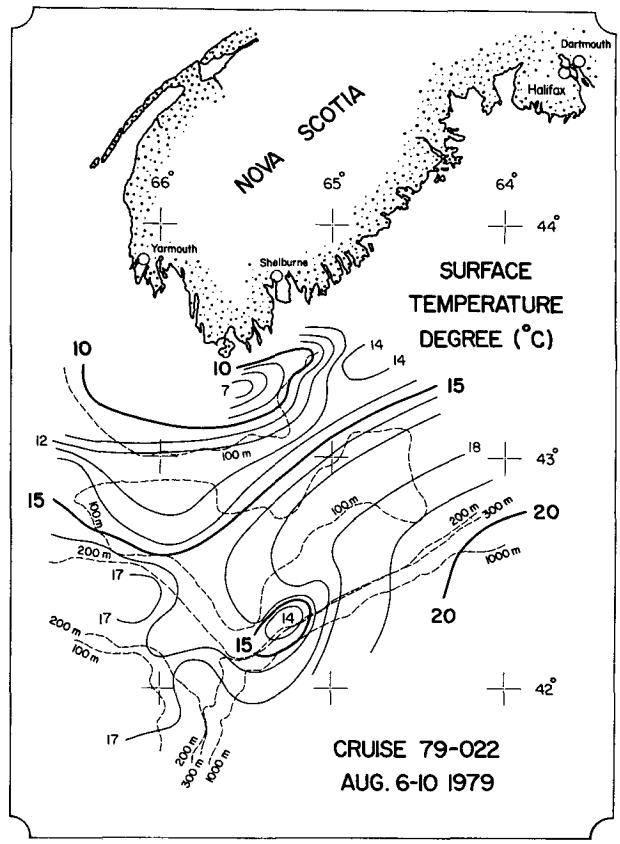

FIG. 10. Observed surface temperature in August 1979, derived from CTD and hull-mounted thermistor measurements. A pronounced cold water anomaly (~7°C) off Cape Sable is indicated.

an estimate of tidal dissipation from the Greenberg et al. (1978) numerical model, Garrett et al. (1978) showed that a transition from well-mixed to stratified conditions (i.e., a "tidal front") in July and August may be delineated by $D/U_m^3 \approx 70\ \mathrm{m^{-2}\,s^3}$, where D is depth of the water column and U_m is the amplitude of the tidal current. Such indications of fronts by D/U_m^3 have been successfully applied to many coastal seas. A more detailed distribution of frontal positions was predicted by Loder and Greenberg (1986) using Greenberg's (1983) fine-grid (~7-km) numerical tidal model. The predicted transition off Cape Sable is shown in Fig. 11 by a thick solid curve. The front near Cape Sable occurs in the vicinity of the 65-m isobath, a finding supported by hydrographic data taken by Fournier et al. (1984) and by the hydrographic sections in Fig. 13b (section II) and Fig. 13c (section III) from this study. The persistence of the well-mixed water throughout the summer in the shallow region has been indicated by the temperature and salinity measurements at various depths at the nearshore current meter station C0 (at 30 m).

Cold surface temperatures can be induced by strong tidal mixing, which blends the surface water with the

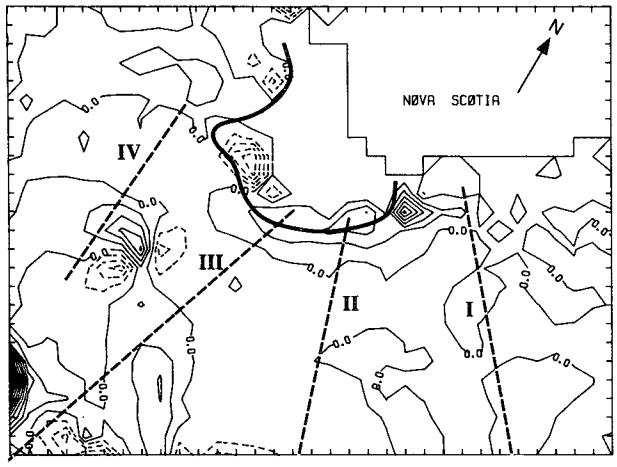

FIG. 11. The superposition of w_2 (10^{-5} m s^{-1}) at 30 m, four hydrographic sections off Cape Sable in 1979 (dotted lines), and predicted frontal location between well-mixed and stratified waters [thick solid curve; Loder and Greenberg (1986)]. See Fig. 3 caption for further details.

colder waters below. To examine whether the cold anomaly in midsummer off Cape Sable can be induced entirely by this mixing (i.e., without advection), we compute the increase of temperature in the well-mixed water during the heating period from spring to summer. For a well-mixed water column with constant thickness D, an increase of temperature (ΔT) by a heat flux on the surface (Q) can be written as (8),

$$\Delta T = \frac{1}{\rho c_p D} \int Q dt, \qquad (14)$$

where t is time, D is water depth, ρ is density, and c_p is the specific heat. Using weather reports from ships and various formulas for radiant, sensible, and latent heat fluxes, Bunker (1976) computed the air–sea heat fluxes over the North Atlantic Ocean. Seasonal variations of the heat fluxes were presented for a number of selected areas. Along the western boundary of the Atlantic Ocean, the areas include both Grand Banks of Newfoundland (~1800 km northeast of Cape Sable) and the Middle Atlantic Bight of the United States (~1400 km southwest of Cape Sable). During spring and summer, the heat fluxes on Grand Bank increase from 152 W m^{-2} in May to a maximum of 174 W m^{-2} in June and decrease to 120 W m^{-2} in August. The variation and magnitude of heat flux in the Middle Atlantic Bight are similar to those on Grand Banks; the heat fluxes increase from 174 W m^{-2} in May to a maximum of 180 W m^{-2} in June and decrease to 104 W m^{-2} in August. The average heat fluxes between May and August in these two areas are about the same (152.0 W m^{-2} on Grand Banks and 152.7 W m^{-2} in the Middle Atlantic Bight), so an averaged heat flux of 152.0 W m^{-2} will be used for computing the temperature variation between May and August around Cape Sable. Note that the heat fluxes southwest of Nova Scotia estimated by Isemer and Hasse [1987; about −150 W m^{-2} in January, +100 W m^{-2} in April, +150 W m^{-2} in July and −50 W m^{-2} in October (charts 25 to 28)] are similar to the variations of heat flux in the Middle Atlantic Bight and Grand Banks area presented by Bunker (1976).

By taking $\rho = 1.024 \times 10^3$ kg m^{-3}, $c_p = 4.0 \times 10^3$ J kg^{-1} °C^{-1}, $Q = 152$ W m^{-2}, and a typical water depth (D) of 40 m off Cape Sable, the increase of temperature [ΔT, Eq. (14)] in a static, well-mixed water column from May to August ($t \sim 120$ days) is 10°C. This would increase the water temperature off Cape Sable from ~4°C in May (Fig. 9) to ~14°C in August. The predicted temperature in August is consistent with the observed temperature in mid-August 1979 in the well-mixed area on the cap of Georges Bank (~15°C; Flagg 1987). The 7°–9°C temperature observed off Cape Sable in August is much lower than this predicted temperature. Thus, tidal mixing alone cannot account for the existence of the cold water anomaly off Cape Sable.

To investigate the process by which the cold water anomaly is formed by the combined actions of tidal mixing and topographic upwelling, we first examine the source of upwelling water. The mean current over the inner half of the Scotian Shelf flows principally in the southwestward direction (the Nova Scotia Current). The water on the eastern side of Cape Sable derives mainly from this southwestward advection of the Scotian Shelf water (Sutcliffe et al. 1976). This shelf water is a mixture of Gulf of St. Lawrence water and more saline slope water. In addition, part of the shelf water near Cape Sable may come from the Gulf of Maine via the tidally induced circulation around Browns Bank (Fig. 2). Most of the transport into the region from the Scotian Shelf and the Gulf of Maine occurs in water deeper (>65 m) than that in the mixing zone (<65 m) near Cape Sable. Because the surface heat flux is approximately uniform over the Scotian Shelf and the Gulf of Maine during the heating season (Bunker 1976; Isemer and Hasse 1987), the increase of the depth-averaged temperature from spring to summer, caused by this heat flux alone, is expected to be smaller in the offshore water than in the shallow region off Cape Sable (14). However, the advection of the offshore water from deep to shallow regions by topographic upwelling on the eastern side of the cape (Figs. 3 to 5) approximately conserves the depth-averaged temperature of the water column [Eq. (13), to be verified in the next subsection]. Thus, the depth-averaged temperature in summer off Cape Sable (~7°C in mid-August) reflects that of the offshore water and is considerably lower than that estimated from the heat flux alone at Cape Sable (~14°C in mid-August).

The cold water in the lower layer of the offshore region, after it has been upwelled into the shallow region, can penetrate efficiently toward the surface layer because of the strong tidal mixing that forms the well-

mixed region near the Cape (Fig. 11). We can see this from the following estimation. By taking the length scale of the shallow area off Cape Sable to be 50 km and the velocity scale of the westward jet to be 0.1 m s^{-1} (Fig. 2), we obtain the time scale for the water parcel to remain in the shallow region to be about 6 days. The mixing time scale can be estimated from D^2/N_m, where D is the depth of shallow region and N_m is the vertical eddy viscosity. The value of N_m is uncertain, but in this study, it is estimated by setting the *magnitude* of the bottom stress in the 3D model to be approximately equal to $\rho\lambda U$, where ρ is density of water, U is the depth-averaged tidal current, and λ is the linear friction coefficient computed from $C_D U_m/D$, where $C_D = 0.0021$ is the drag coefficient, U_m is the magnitude of tidal current, and D is depth (Tee 1979, 1980). The estimation of N_m is related to flow field (U_m) and topographic variation (D). Near Cape Sable, this value is $\sim$0.03 $m^2 s^{-1}$, smaller than the value proposed by Bowden (1967) [$N_m = 0.10$ $m^2 s^{-1}$ computed from $2.5 \times 10^{-3} U_m D$ with $U_m \sim 1.0$ m s^{-1} and $D \sim 40$ m (shallow area)], and about the same as that proposed by Csanady (1976; $N_m = 0.026$ $m^2 s^{-1}$ computed from $0.1 C_D U_m^2/20f$, where $f = 10^{-4}$ s^{-1}). If we take the lower limit of N_m ($\sim$0.03 $m^2 s^{-1}$) and the depth of $\sim$40 m in the well-mixed area off Cape Sable, we obtain the mixing time scale of 0.6 days. This mixing time scale, consistent with that predicted on Georges and Browns banks (Loder et al. 1988), is an order of magnitude smaller than the advective time scale. Thus, the water parcel in the lower layer can be efficiently transported into the surface layer, resulting in the observed cold surface water near Cape Sable.

The presence of several ridges west of Cape Sable cannot explain the occurrence of the cold water anomaly in the Cape Sable area. This is because the ridges are located within the 40-m isobath contour in the well-mixed area (see the Canadian Hydrographic Chart 10590; note that the density front is located at about the 65-m isobath). As the water is already well mixed, the additional vertical mixing on the shallow ridge does not affect the vertical temperature distribution in the water column. In fact, the water on the shallow ridge is expected to be warmer than the surrounding deep water in midsummer because the temperature increase in a well-mixed water column during the warming season is inversely proportional to depth [Eq. (8)]. Furthermore, the ridges are about 20 km away from the density frontal region (at about 65-m isobath), and significantly away from the influence of the tidal advection of stratified water (tidal excursion is about 10 km).

The numerical tidal model also predicts other areas of topographic upwelling (Figs. 3–5; section 2). One of these areas is Browns Bank. A small well-mixed area ($\sim$7 km in diameter) over the cap of Browns Bank was also predicted by Loder and Greenberg (1986). However, this well-mixed area in summer was not detected in hydrographic data or satellite imagery. This disagreement was attributed to the smallness of the area (Loder and Greenberg 1986). Because the local tidal excursion is comparable to the size of the predicted well-mixed area, no single water column spends enough time in the area of strong mixing on Browns Bank to remain well mixed. The absence of a well-mixed zone also explains the absence of low surface temperatures on Browns Bank (Figs. 10 and 13c).

Strong topographic upwelling and downwelling are also predicted on the southern corner of the model (Figs. 3–5). The reliability of these vertical velocities requires some further studies because of the uncertainty in the model predictions near open boundaries.

c. *Conservation of depth-averaged temperature*

The conservation of depth-averaged temperature during the topographic upwelling process involves two approximations (section 3). The first is that the depth-average of $\mathbf{u}_2 T$ (denoted by $\langle \mathbf{u}_2 T \rangle$) can be approximated by $U_2 \tilde{T}$, where u_2 is the three-dimensional tidally induced residual current, T is the temperature, and U_2 and $\tilde{T}$ are the depth-averaged values of u_2 and T. The second is that the time scale for the upwelling, which can be approximated by the cross-isobath advective time scale, is much shorter than the period of the heating season. The validity of these two approximations is now examined.

The accuracy of the first approximation can be estimated from

$$|\delta M| = |\langle \mathbf{u}_2 T \rangle| - |\mathbf{U}_2 \tilde{T}| \qquad (15)$$

and

$$\delta\theta = \text{direction of } \langle \mathbf{u}_2 T \rangle - \text{direction of } \mathbf{U}_2 \tilde{T}, \qquad (16)$$

where $\delta M = \langle \mathbf{u}_2 T \rangle - \mathbf{U}_2 \tilde{T}$, and $|\delta M|$ and $\delta\theta$ measure the errors in the magnitude and direction of the approximation. By dividing both sides of (15) by $|U_2 \tilde{T}|$, we can measure the magnitude error in terms of temperature,

$$\delta T = (\hat{T} - \tilde{T})/\tilde{T}, \qquad (17)$$

where $\hat{T} = |\langle \mathbf{u}_2 T \rangle|/|\mathbf{U}_2|$ and $\delta T = |\delta M|/|\mathbf{U}_2 \tilde{T}|$. An example of the vertical profile of temperature, salinity, and residual currents at station 12 on the eastern side of Cape Sable (Fig. 8) is shown in Fig. 12. Despite the stratification of the water column at this station, it was found that $\langle \mathbf{u}_2 T \rangle$ could be approximated accurately by $\mathbf{U}_2 \tilde{T}$ because the residual current varies weakly in the water column. The good approximation is shown by small values of δT [-1.1% or $(\hat{T} - \tilde{T}) = -0.08$°C] and $\delta\theta$ (-1.5°C). Similar results are obtained for other stations southwest of Nova Scotia. The averaged values of $|\delta T|$ and $|\delta\theta|$ for all the stations near Cape Sable (stations 7 to 12, and 21 to 24; Fig. 8) are 0.9% [or $(\hat{T} - \tilde{T}) \sim 0.07$°C] and 1.9°. Comparable results are found for salinity and nitrate (9). As an example, the

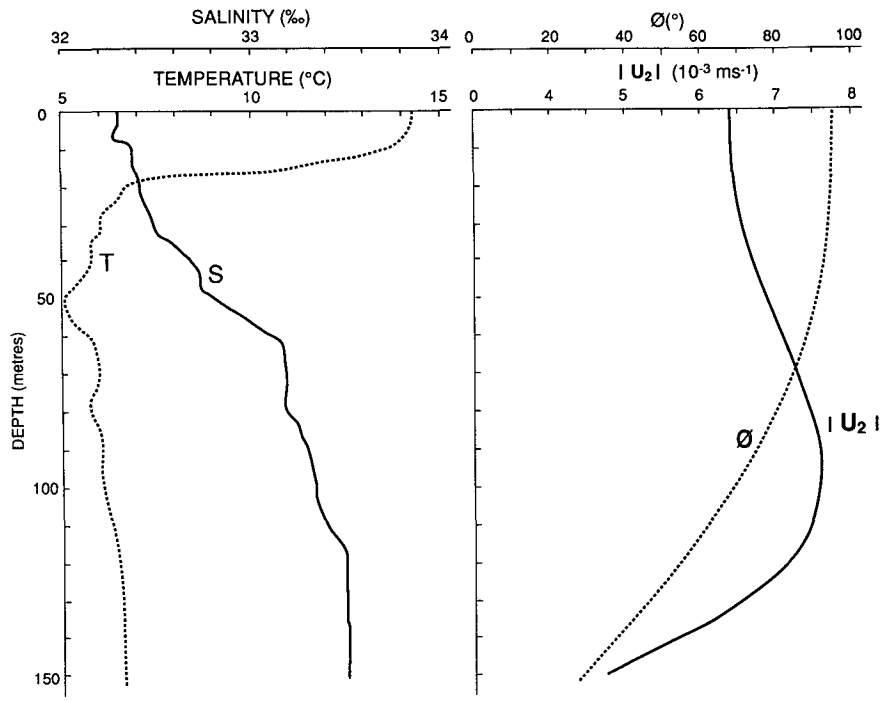

FIG. 12. The vertical distribution of (a) observed temperature (solid) and salinity (dashed) and (b) computed magnitudes (solid) and directions (dashed) of the tidally induced residual current at station 12 on the eastern side of Cape Sable (see Fig. 8). The observation was taken on 7 August 1979. Directions of the residual current are measured clockwise from true North.

averaged errors of the approximation in salinity for the stations near Cape Sable are 0.04% in magnitude (or 0.01 ppt in salinity) and 0.08° in direction.

The approximation of the depth-averaged temperature equation (8) can be examined in more detail by estimating the term $D^{-1}\nabla \cdot D\delta M$ neglected in the equation. The length scale of δM is found to be the same order as the topographic length scale $L_t[=(D^{-1}\nabla \cdot D)^{-1}]$. By computing the value of δM from $|\mathbf{U}_2|(\hat{T}-\tilde{T})$, the neglected term can be estimated from $|\mathbf{U}_2|(\hat{T}-\tilde{T})/L_t$. From the averaged cross-isobath residual current ($|\mathbf{U}_2|$) of 0.009 m s^{-1} at the 60-m isobath east of Cape Sable, the topographic length scale (L_t) of 15 km, and the average $(\hat{T}-\tilde{T}) \approx 0.07$°C, we find the neglected term to be 4.2×10^{-8} °C s^{-1}. By using the averaged heat flux on the surface (Q) to be 152 W m^{-2}, the density of water (ρ) to be 1.024×10^3 kg m^{-3}, the specific heat (c_p) to be 4.0×10^3 J kg^{-1} °C^{-1}, and the depth of the water column (D) to be 60 m, the seasonal heating term in (8), $Q/(\rho c_p D)$, is 6.2×10^{-7} °C s^{-1}. Thus, the neglected term in Eq. (8) is about an order of magnitude smaller than the seasonal heating term. Note that, during the cross-isobath advection of water parcels, the contribution of the heating term to the depth-averaged temperature is already quite small (see the next paragraph).

To justify the second approximation of a short advective time scale, we use the average cross-isobath residual current at 60 m in the upwelling area (~0.009 m s^{-1}) and the isobath separation between 40 and 80 m (~10 km) to obtain the scale of 12.9 days. This time scale is about an order of magnitude smaller than the heating period from April to August (~120 days). For the average heat flux of 152 W m^{-2} in the Cape Sable area in spring and summer, and the average water depth of (D_A) 60 m, the depth-averaged temperature of the upwelling water in the shallow region [$\tilde{T}_{n+1}$(shallow)] increases by about 0.7°C over the period of advection (11). If the water column remains offshore at 80 m (D_p), the temperature in deep water [$\tilde{T}_{n+1}$(deep)] would increase by 0.53°C (12). This increase of temperature (0.17°C) due to the change of water depth over the period of cross-isobath advection is very small in comparison to the increase of the depth-averaged temperature near Cape Sable over the heating season (~4° to 6°C).

d. Evidence of the topographic upwelling from the hydrographic data

The important feature of the predicted topographic upwelling is that it occurs mainly on the eastern side of Cape Sable. This feature is now verified by examining the offshore sources of cold water. Of the four 1979 hydrographic sections (Fig. 8), sections I and II are on the eastern side of the Cape, whereas sections III and IV are on the southern and western sides. The water on the Scotian Shelf (section I, Fig. 13a; see Fig. 8 for

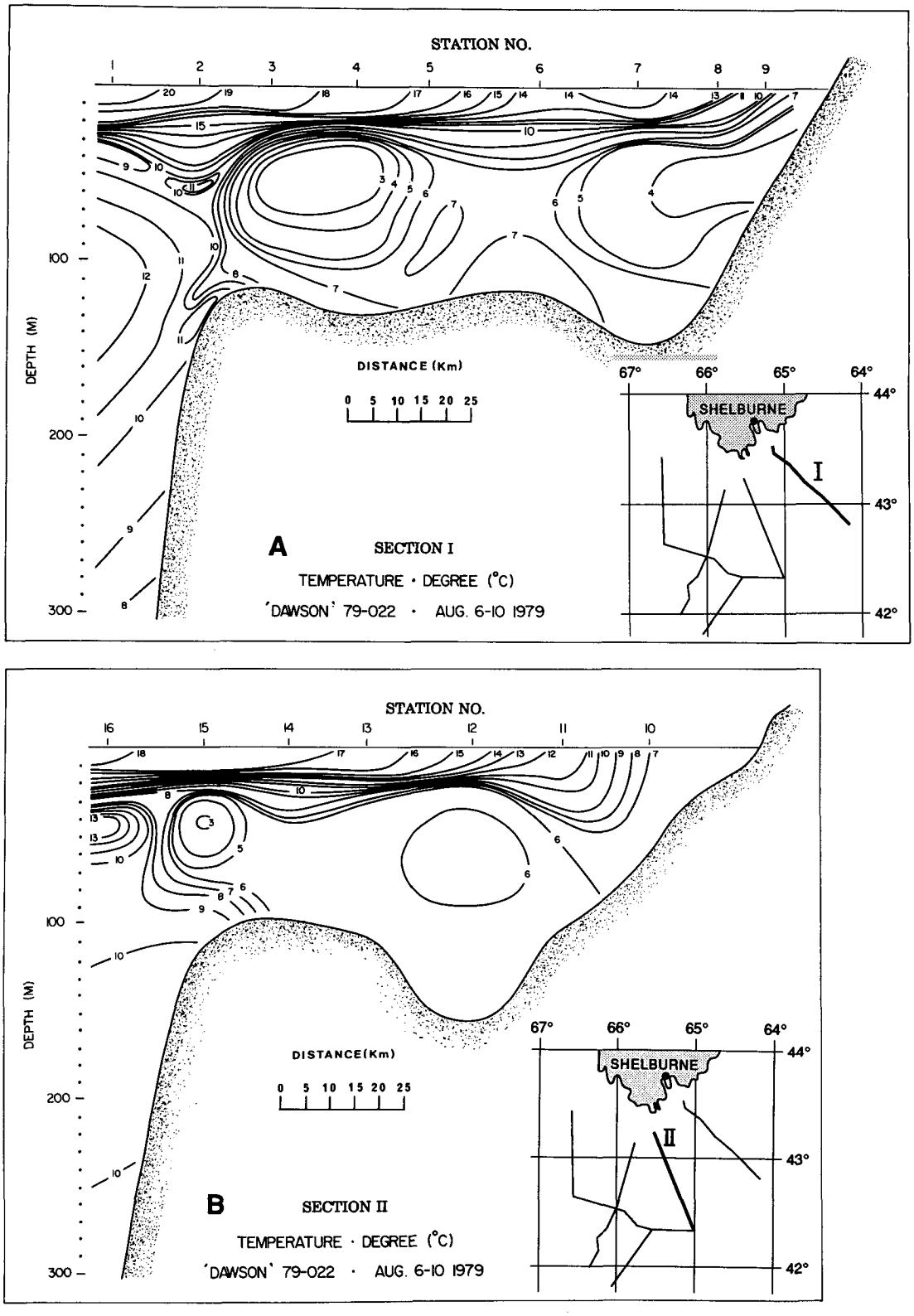

FIG. 13. The temperature variation along (a) section I, (b) section II, (c) section III, and (d) section IV in the Cape Sable area. The labels in the x axis are the station numbers (see Fig. 8).

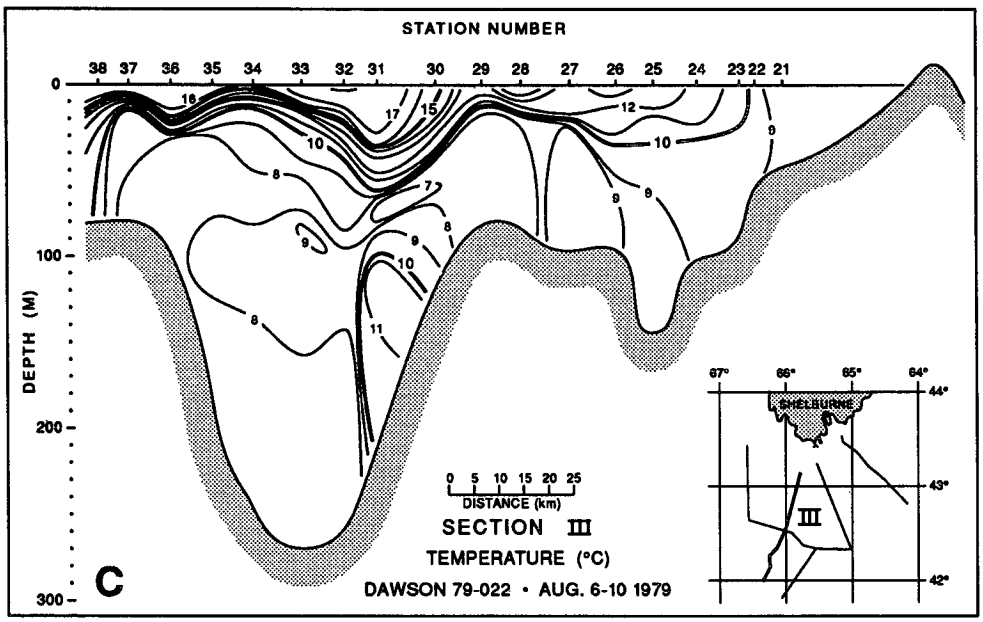

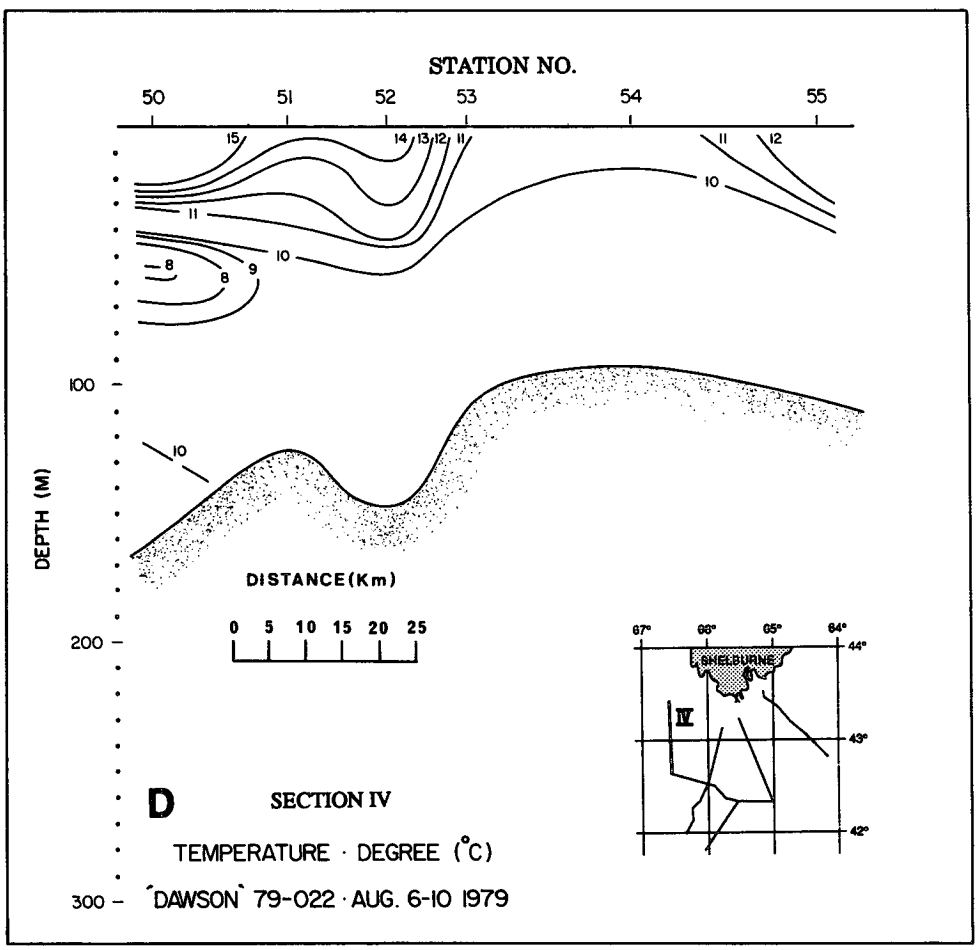

FIG. 13. (*Continued*)

station numbers) is thermally stratified, with the temperature decreasing from the surface to a minimum at intermediate depths. The warm surface layer extends entirely across the shelf with the surface temperature increasing offshore from 10°C at the nearshore station to about 19°C at the shelf break. The cold intermediate layer is located a depth at around 60 m, and has a minimum temperature of ~3°C. The cold water off Cape Sable can be supplied by this cold intermediate layer.

On the inner shelf of section II, the lower layer of the water column is well mixed with a temperature of ~6°C. The front between the well-mixed and stratified regions is located between the two stations nearest shore, stations 10 and 11. The water masses at station 10 were more or less well mixed with the temperature around 6°–7°C, and those at station 11 were stratified. The cold temperature of ~7°C in the well-mixed area near Cape Sable is close to that in the lower layer of the offshore stratified water (~6°C).

On section III, south of Cape Sable (Fig. 13c), the well-mixed water of 9°C is observed at the station nearest to the shore (station 21). This temperature is very close to those in the lower layer at offshore stations 22 to 27, which agrees with the prediction of the topographic upwelling in the area. This temperature is about 2°C warmer than the minimum temperature observed near Cape Sable, which suggests that the cold anomaly (~7°C) near the Cape does not originate in the lower layer of this section. Also, the strong westward currents near Cape Sable (Fig. 2) prevent the advection of the upwelling water to the cold anomaly area. The "recycled" waters from the westward jet through the cyclonic residual eddy on the southeastern side of the jet and the northward flow from the northern flank of Browns Bank are probably the major contributors to the 9°C waters on this section (Fig. 2).

On section IV, located west of Cape Sable (Fig. 13d), the predominant temperature in the lower layer is 10°C except in the cold intermediate layer at the southernmost station, which has a minimum of 8°C.

The comparison of temperature in the lower layer near the frontal region between various hydrographic sections (Fig. 13) indicates that the temperature increases westward toward the Gulf from 4°C at section I, to 6°C at section II, 9°C at section III, and 10°C at section IV. The combination of 1) this temperature variation, which shows the existence of cold water (<7°C) on the eastern sections (I and II), 2) the observed temperature front, which shows the well-mixed water shallower than 65 m, and 3) the topographic upwelling, predicted to be mainly on the eastern side of Cape Sable (Fig. 11), strongly support our suggestion that the cold anomaly (7°C) off Cape Sable is induced by the combined action of topographic upwelling and tidal mixing.

The origin of the cold water mass near Cape Sable can be studied in more detail by including the salinity distribution, in particular by examining the depth-averaged temperature ($\tilde{T}$) and salinity ($\tilde{S}$, section 3). The distribution of $\tilde{T}$ and $\tilde{S}$ for the nearshore stations on the four hydrographic sections (Fig. 14) indicates that the anomalously cold water mass in the well-mixed region off Cape Sable has a temperature of ~7°C and salinity of ~32.65 psu (station 10). This $\tilde{T}$–$\tilde{S}$ characteristic can be formed approximately by mixing the water column at nearby stations 7 and 8 on section I and stations 11 and 12 on section II on the eastern side of Cape Sable. On the other hand, the mixing of the water column at nearby stations on sections III (stations 21–25) and IV (stations 52–55) on the southern and western sides of the Cape produces a warmer and/or saltier water mass than that at station 10. This result shows that the cold water off Cape Sable originates mainly from the eastern side of the Cape, consistent with the model prediction.

Figure 14 also shows that the depth-averaged salinity and temperature at station 9 (32.0 psu and 5.1°C) are much fresher and colder than those at station 10 (32.65 psu and 7°C). Thus, the cold water mass at station 10 is not controlled by the advection of Scotian Shelf water from station 9 (along the 60-m isobath) where the southwestward alongshore currents have been observed (Smith 1983). [The currents measured at C5 and C6 (Fig. 2) near station 9 are probably induced by wind and buoyancy forcing, which are not included in the model.] One possible reason for the small contribution by alongisobath flow is that part of the shelf water advected southwestward from station 9 is diverted to the inshore shallow region by the tidally induced residual currents (Fig. 2). Another reason may be that the volume transport of the alongisobath inshore flow is significantly smaller than that induced by topographic upwelling on the eastern side of Cape Sable. The total cross-isobath volume transport by upwelling at the 60-m isobath was found to be $\sim 5 \times 10^4$ m^3 s^{-1}. The southwestward advection of shelf water can be estimated by using the observed longshelf current (~0.04 m s^{-1}) at current meter station C5. By assuming that

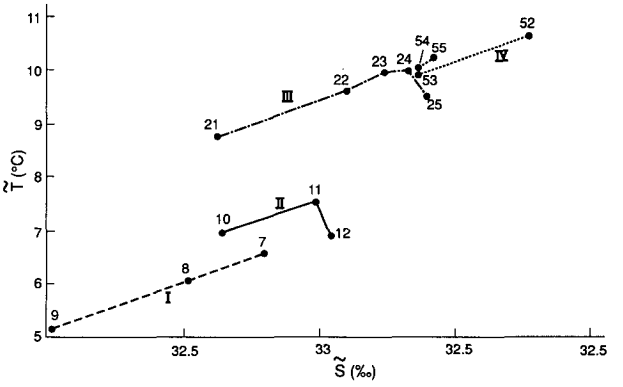

FIG. 14. The depth-averaged temperature ($\tilde{T}$) and salinity ($\tilde{S}$) at the hydrographic stations on sections I (dashed), II (solid), III (dash-dotted), and IV (dotted) near Cape Sable. The station numbers are shown near the data (solid dots).

the current decreases linearly to zero at the coast, the total volume transport within the 60-m isobath is approximately 10^4 m^3 s^{-1}, about 20% of the transport by topographic upwelling. The percentage may be significantly lower in summer because the longshore current near the Nova Scotia coast during this season, in response to the upwelling-favorable wind (northeastward alongshore component), has been found to be in the northeastward direction (Petrie et al. 1987).

The continuous supply of nutrients from lower to upper layers by the combined effects of topographic upwelling and tidal mixing is expected to produce high nutrient concentrations in the well-mixed area off Cape Sable. Figure 15 shows high nitrate concentration in the well-mixed water at nearshore stations on section II and the depletion of nitrate in the surface layer on section I. The nitrate values in the shallow region of section III are similar to those on section II. High nitrate concentration in the well-mixed area in summer 1977 has also been observed by Fournier et al. (1984). To explore the possible advection of nitrate from the offshore deep to inshore shallow regions, we examine the horizontal distribution of the depth-averaged nitrate concentration [$\tilde{C}$; Eq. (9)]. The value of $\tilde{C}$ at station 10 in the shallow region (6.30 μM) is comparable to those at stations 7 (8.12 μM), 8 (6.62 μM), 11 (6.79 μM), and 12 (9.24 μM) in the deep regions. A comparison with Georges Bank suggests that the high nitrate concentration in the well-mixed region off Cape Sable in mid-August is not due to the tidal mixing alone. In the well-mixed area on the cap of Georges Bank, the absence of the topographic upwelling is indicated by the high temperature ($\sim$15°C) in mid-August (Flagg 1987). The high levels of primary production in spring substantially reduced nitrate concentrations in this area [from 4–6 μM in April to less than 1.0 μM between May and October; O'Reilly et al. (1987)]. However, in the well-mixed area off of Cape Sable, the nitrate concentration in mid-August is high ($\sim$6 μM) and is found to be comparable to those values measured in April (2–4 μM) and November (7–10 μM). This result indicates both the existence of topographic upwelling off Cape Sable and the importance of the upwelling to the renewal of nitrate concentration. Furthermore, the close agreement between the depth-averaged nitrates in the shallow and deep regions suggests that biological uptake rates are not significant, so that nitrate concentration may be treated as a conservative property over the upwelling time scale. This is plausible since the nutrient rich deep water is removed from the photic zone until mixed upward by the tide in shallow water, where its exposure is then limited by the mixing itself (Fournier et al. 1984).

e. *Evidence of the topographic upwelling from current meter observation*

Because topographic upwelling and downwelling are closely related to horizontal structure of the residual current (Fig. 7), they can be verified by comparing the computed and observed horizontal residual circulations. The current meter mooring array consists of a line of five sites (C0 to C4) along section III, and two more sites (C5, C6) along section I (Fig. 11). The comparison between predicted (Fig. 2) and observed residual currents, which requires the estimation of the tidally induced component of the residual current from the current meter data, was performed by Tee et al. (1988) using a multiple regression technique. The results showed that the estimation had large uncertainty (signal less than twice the 95% confidence limits) for most of the current meter records. Near Cape Sable, only the estimation at station C0 had a high signal-to-noise ratio (signals are about 4.4 times the confidence limit). Three current meters (15, 22, and 25 m below the surface) were moored at this station for periods of 13, 17, and 17 months, respectively. Both model and observed residual currents vary weakly over the water column: the estimated residual currents decrease from 0.272 m s^{-1} at 15 m to 0.205 m s^{-1} at 25 m, and the model currents decrease from 0.217 m s^{-1} to 0.186 m s^{-1} over the same depths. The directions of the estimated residual current decrease slightly from 257° (measured clockwise from true north) at 15 m to 247° at 25 m, while the model currents are more or less constant at 258°. The averaged current over the three estimated values (solid arrow) is compared in Fig. 2 to the model results for the depth-mean residual current. We can see that the observed tidally induced residual currents at station C0 are very well reproduced by the three-dimensional numerical tidal model. This result indicates that the numerical simulations of topographic upwelling and downwelling near Cape Sable are reasonably reliable.

f. *Evidence of the topographic upwelling from Lagrangian drift data*

Between April 1983 and May 1985, estimates of the Lagrangian surface circulation in the vicinity of southwest Nova Scotia have been obtained by tracking clusters of drogued (10-m) satellite beacons (Fig. 16a) that were deployed at various times and locations on Browns Bank (Smith 1989a). Subsequent positions of the buoys were obtained via the ARGOS satellite system, with a relative accuracy of 200 m. Drift tracks for selected deployments (Fig. 16b) reveal the tendency of the drogues to follow the tidally induced anticyclonic gyre on Browns Bank and exit the bank along its northern flank. In some cases, a strong pulse of wind seemed to assist the drifters to leave the bank, but even in the absence of wind, escape to the north was consistently observed.

A summary of the Lagrangian surface circulation, based on averages of all drift measurements in all seasons (Fig. 16c), reflects both the Browns Bank gyre and the strong offbank flow to the north. The average velocities were determined from drogue displacement

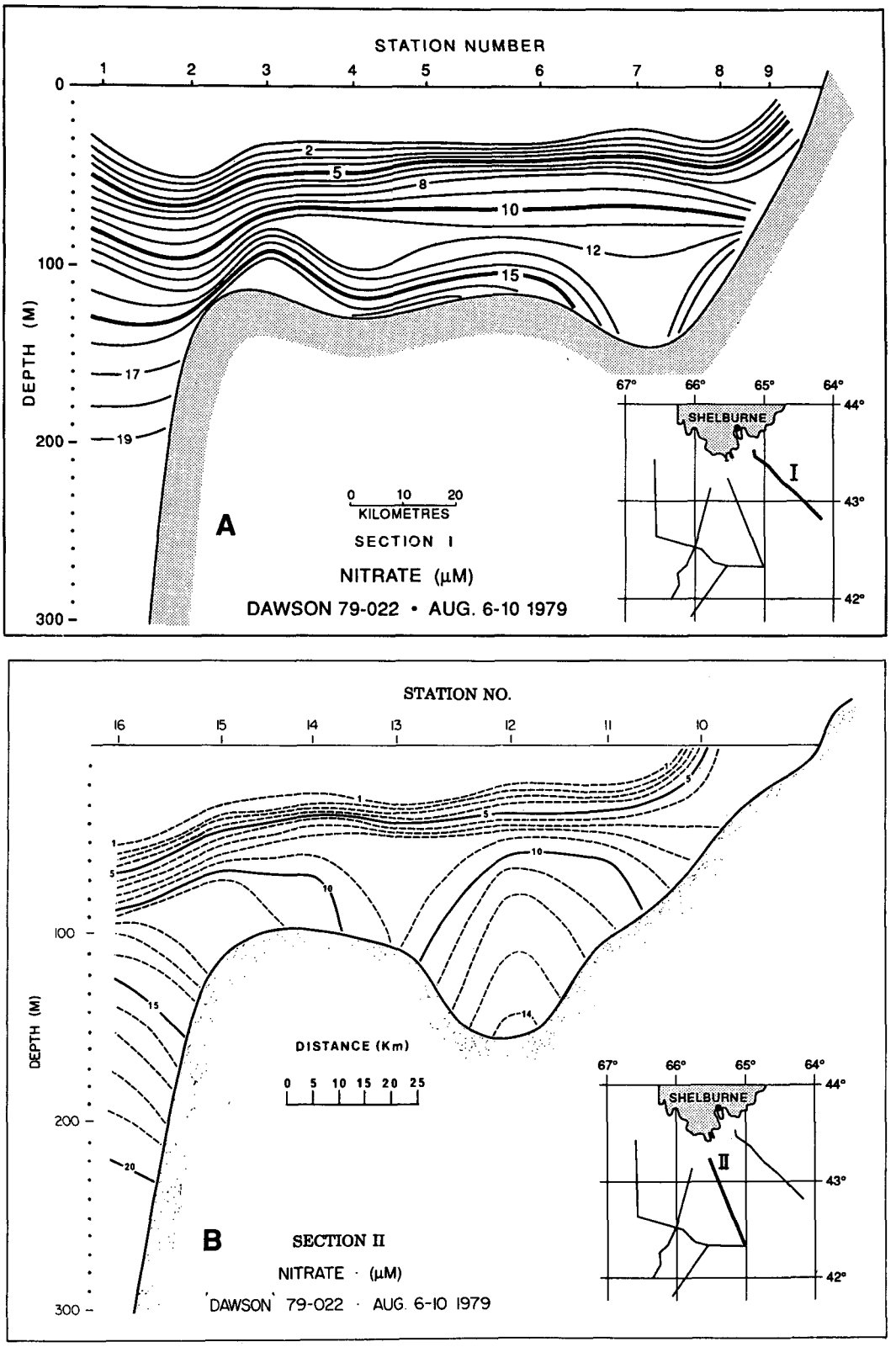

FIG. 15. Nitrate concentration on (a) section I and (b) section II taken on 7 August 1979. The figure shows high concentration in the well-mixed area on section II, and the depletion of nitrate in the surface layer on section I.

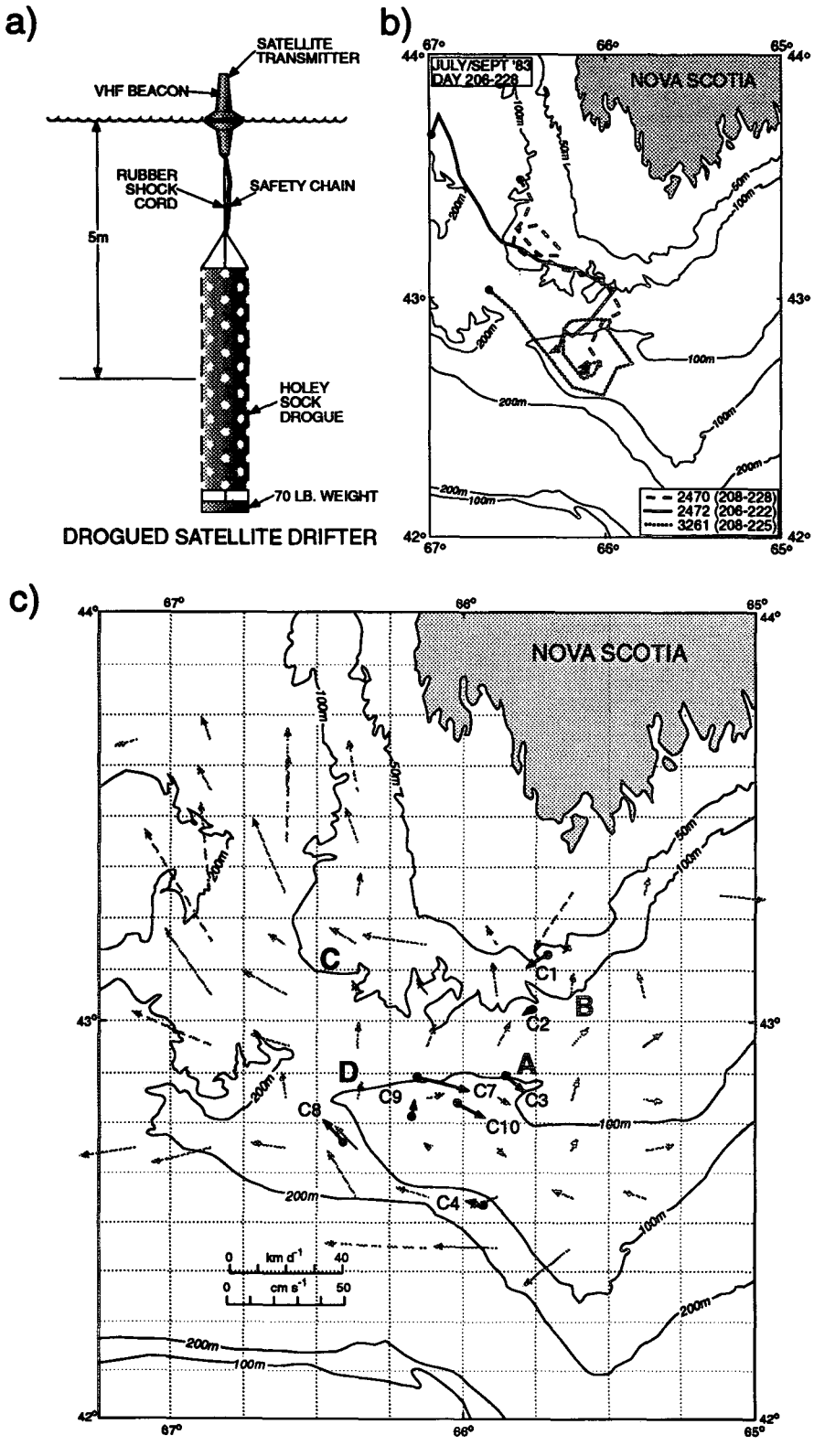

FIG. 16. Lagrangian drift measurement taken between April 1983 and May 1985: (a) structure of the drogued satellite drifter, (b) an example of drifter tracks taken between July and September 1983, and (c) the averaged Lagrangian surface currents (dashed arrows) and the measured Eulerian residual currents (solid arrows).

rates on a $1/8° \times 1/4°$ grid. In the central portion of the grid (42°30′ to 43°N, 65°30′ to 66°30′W) the number of independent estimates in each average ranged from 10 to 96, and the standard deviations of the Lagrangian speeds were typically comparable to the mean speeds. The estimated Lagrangian currents generally agree with the measured Eulerian residual currents in the area. This result is consistent with the model output that shows that the overall Eulerian and Lagrangian components of the tidally induced residual circulation within the area between Browns Bank and the westward jet are generally similar. Also, because the tidally induced residual currents are only weakly sheared, the surface circulation can be used to indicate the circulation throughout the water column. We can, therefore, compare qualitatively the Eulerian depth-averaged residual circulation (Fig. 2) and the observed Lagrangian surface circulation.

On the northeastern side of Browns Bank (near location A, Fig. 16c), the water parcels move northeastward off the bank. These parcels subsequently cross isobaths from deep to shallow water toward Cape Sable (near location B). This flow structure is consistent with the tidally induced anticlockwise residual gyre on the southern side of the westward jet. The observed cross-isobath flow near Cape Sable supports our conclusion that the topographic upwelling occurs on the eastern side of the cape, and is induced by the water parcels moving from deep to shallow waters.

The westward flow of the jet near location C (Fig. 16c) is also indicated by the Lagrangian drift measurements. However, the model's southward flow near the northwestern tip of Browns Bank contrasts with the observed northward flow near location D. The reason for this discrepancy is unclear, but it may be related to the baroclinic circulation in the deep central region of the Gulf of Maine.

5. Summary and conclusions

The upwelling off Cape Sable, southwest of Nova Scotia, has been studied using a three-dimensional tidal model developed by Tee (1979, 1980, 1987) and field observations carried out between 1978 and 1985. The field program included current meter moorings, hydrographic surveys, and Lagrangian drifter measurements.

The numerical model predicts several areas of strong upwelling and downwelling. Off Cape Sable upwelling occurs on the eastern side, and downwelling on the western side (Fig. 3) with maximum values of order 10^{-4} m s^{-1}. The upward vertical transport is very significant in supplying cold, saline, and nutrient-rich water from deep to shallow regions.

The predicted upwelling and downwelling are induced by a tidal rectification process resulting from tidal currents flowing over complex bottom topography. Because the vertical residual currents are induced by topographic rectification, they are named "topographic upwelling and downwelling." These processes are expected to be important in other coastal areas where strong tidal currents and significant variations of bottom topography exist.

The topographic upwelling and downwelling result from residual currents that cross isobaths. The upwelling (downwelling) is generated by the residual currents flowing from deep to shallow (shallow to deep) water. The convergence or divergence of this cross-isobath flow is compensated by the divergence or convergence of the alongisobath residual current. Thus, the topographic upwelling process is three dimensional, as opposed to classical two-dimensional upwelling that features onshore flow in the lower portion of the water column and offshore flow in the upper portion. The two-dimensional circulation provides efficient transport of cold, saline, and nutrient-rich water from lower to surface layers. However, in three-dimensional topographic upwelling, the water parcels in the lower layer do not have to form an offshore return flow, but rather they may remain in the lower layer and be advected away from the upwelling region by longshore coastal currents. Thus, the upward transfer of cold and saline water associated with topographic upwelling may not be as efficient as in the two-dimensional case. However, the vertical exchange can be accomplished by another mechanism if the cross-isobath transport associated with the upwelling carries the deep water to a region that is sufficiently shallow and has strong tidal currents. In such areas, the vertical mixing from the turbulence generated by tidal currents at the bottom can efficiently transfer water parcels from lower to surface layers. This combination of topographic upwelling and strong tidal mixing is the mechanism that produces the observed cold-water anomaly off Cape Sable (about 7°C in mid August). The upwelling there occurs mainly on the eastern side of the cape, and the strong tidal mixing produces a well-mixed area off the cape. The existence of this mechanism for producing cold water is supported by the hydrographic, current meter, and Lagrangian drift data collected in the Cape Sable area between 1978 and 1985.

Acknowledgments. The authors thank Dr. C. J. R. Garrett of the University of Victoria, and Dr. R. A. Clarke of the Bedford Institute of Oceanography for their critical review and valuable suggestions. We also thank two anonymous reviewers for their valuable comments.

APPENDIX

Relationship between Depth-averaged Vertical Velocity and Cross-Isobath Residual Current

For a Cartesian system with horizontal coordinates x, y and vertical coordinate z, measured vertically up-

ward from the mean sea level, the continuity equation for the residual currents is

$$\frac{\partial w_2}{\partial z} + \nabla \cdot \mathbf{u}_2 = 0, \tag{A1}$$

where $\mathbf{u}_2$ and w_2 are the horizontal and vertical residual currents. From (A1), w_2 can be computed from

$$w_2 = w_{2D} - \int_{-D}^{z} \nabla \cdot \mathbf{u}_2 dz', \tag{A2}$$

where w_{2D} is the vertical velocity at the bottom. Because the tidally induced residual current above the bottom boundary layer generally varies gently over the water column (Tee et al. 1987; also see Fig. 12), we assume to first order that u_2 is uniform over the water column and given by the depth-averaged value (U_2). At the bottom, the residual flow is assumed to be parallel to the bottom,

$$w_{2D} = -\mathbf{U}_2 \cdot \nabla D. \tag{A3}$$

From the continuity equation of the depth-averaged residual current,

$$\nabla \cdot (D\mathbf{U}_2 + \overline{\zeta_1 \mathbf{u}_{10}}) = 0, \tag{A4}$$

we obtain

$$\nabla \cdot \mathbf{U}_2 = -[(\mathbf{U}_2 \cdot \nabla D) - w_{2o}]/D, \tag{A5}$$

where $\underline{U_2}$ is the depth-averaged residual current, $w_{2o} = \nabla \cdot \overline{\zeta_1 \mathbf{u}_{10}}$ is the value of w_2 at the surface (Tee 1993), and $\mathbf{u}_{10}$ is the value of $\mathbf{u}_1$ at the surface. By neglecting the small vertical velocity at the surface ($w_{2o} \approx 0$), w_2 can be computed from (A2), (A3), and (A5) as

$$w_2 = D^{-1}(\mathbf{U}_2 \cdot \nabla D)z. \tag{A6}$$

Equation (A6) shows that w_2 decreases from $-\mathbf{U}_2 \cdot \nabla D$ at the bottom to zero at the surface, which qualitatively describes the increase of the model's w_2 in the deeper portion of the water column (Figs. 3 and 7). The depth average of w_2, computed from (A6), becomes

$$W_2 = -\frac{1}{2}\mathbf{U}_2 \cdot \nabla D. \tag{A7}$$

Thus, the computed $(-\mathbf{U}_2 \cdot \nabla D)$ is about twice of W_2 [Eq. (1)].

REFERENCES

Bailey, W. B., W. Templeman, and R. P. Hunt, 1954: The horizontal distribution of temperatures and salinities off the Canadian Atlantic Coast. *Fish. Res. Board Can., MS Rep. Ser. (biol)*, **584**, 21 pp.

Bowden, K. F., 1967: Stability effects on turbulent mixing in tidal currents. *Phys. Fluid*, **10**(Suppl.), S278–280.

Bumpus, D. F., and L. M. Lauzier, 1965: Surface circulation on the continental shelf off eastern North America between Newfoundland and Florida. *Folio 7, Serial Atlas of the Marine Environment*, Amer. Geogr. Soc.

Bunker, A. F., 1976: Computations of surface energy flux and annual air–sea interaction cycles of the North Atlantic Ocean. *Mon. Wea. Rev.*, **104**, 1122–1140.

Csanady, G. T., 1976: Mean circulation in shallow seas. *J. Geophys. Res.*, **81**, 5389–5399.

Davis, A. M., 1980: Application of the Galerkin method to the formulation of a three-dimensional nonlinear hydrodynamic numerical sea model. *Appl. Math. Modelling*, **4**, 245–256.

Flagg, C., 1987: Hydrographic structure and variability. *Georges Bank*, R. H. Backus and D. W. Bourne, Eds., 108–124.

Flather, R. A., and N. S. Heaps, 1975: Tidal computation for Morecambe Bay. *Geophys. J. R. Astron. Soc.*, **42**, 489–517.

Fournier, R. O., J. Marra, R. Bohrer, and M. Van Det, 1977: Plankton dynamics and nutrient enrichment of the Scotian Shelf. *J. Fish. Res. Board Can.*, **34**, 1004–1018.

——, M. Van Det, N. B. Hargraves, J. S. Wilson, T. A. Clair, and R. Ernst, 1984: Physical factors controlling summer distributions of chlorophyll *a* off southwestern Nova Scotia. *Limnol. Oceanogr.*, **29**, 517–526.

Garrett, C. J. R., and R. H. Loucks, 1976: Upwelling along the Yarmouth shore of Nova Scotia. *J. Fish. Res. Board Can.*, **33**, 116–117.

——, J. R. Keeley, and D. A. Greenberg, 1978: Tidal mixing versus thermal stratification in the Bay of Fundy and Gulf of Maine. *Atmos.-Ocean*, **16**, 403–423.

Greenberg, D. A., 1979: A numerical model investigation of tidal phenomena in the Bay of Fundy and Gulf of Maine. *Mar. Geol.*, **2**, 161–187.

——, 1983: Modeling the barotropic circulation in the Bay of Fundy and Gulf of Maine. *J. Phys. Oceanogr.*, **13**, 888–906.

Holloway, P. E., 1981: Longitudinal mixing in the upper reaches of the Bay of Fundy. *Estuarine Coastal Shelf Sci.*, **13**, 495–515.

Isaji, T., and M. L. Spaulding, 1984: A model of the tidally induced residual circulation in the Gulf of Maine and Georges Bank. *J. Phys. Oceanogr.*, **14**, 1119–1126.

Isemer, H.-J., and L. Hasse, 1987: *The Bunker Climate Atlas of the North Atlantic. Vol. 2: Air–Sea Interactions*. Springer-Verlag, 251 pp.

Kohler, A. C., 1968: Fish stocks of the Nova Scotia Banks and Gulf of St. Lawrence. Fish. Mar. Serv. Res. Dev. Tech. Rep. 80, 27 pp.

Lauzier, L. M., 1967: Bottom residual drift on the continental shelf area of the Canadian Atlantic Coast. *J. Fish. Res. Board Can.*, **24**, 1845–1858.

Lively, R. R., 1984: Current meter, meteorological, and sea-level observations off Cape Sable, Nova Scotia. Can. Tech. Rep. Hydrogr. Ocean Sci., 40, 494 pp.

——, 1985: Current meter, meteorological, and sea-level observations off Cape Sable, Nova Scotia, August 1980 to April 1983. Can. Tech. Rep. Hydrogr. Ocean Sci., 66, 528 pp.

Loder, J. W., and D. A. Greenberg, 1986: Predicted positions of tidal fronts in the Gulf of Maine region. *Contin. Shelf Res.*, **6**, 397–414.

——, C. K. Ross, and P. C. Smith, 1988: A space- and time-scale characterization of circulation and mixing over submarine banks with application to the northwestern Atlantic continental shelf. *Can. J. Fish. Aquat. Sci.*, **45**, 1860–1885.

Nihoul, J. C. J., and F. C. Ronday, 1975: The influence of the "tidal stress" on the residual circulation, *Tellus*, **5**, 484–489.

O'Reilly, J. E., C. Evans-Zetlin, and D. A. Busch, 1987: Primary Production. *Georges Bank*, R. H. Backus and D. W. Bourne, Eds., The MIT Press, 220–233.

Petrie, B., B. J. Topliss, and D. G. Wright, 1987: Coastal upwelling and eddy development off Nova Scotia. *J. Geophys. Res.*, **29**, 12 979–12 991.

Pingree, R. D., and L. Maddock, 1977: Tidal residual in the English Channel. *J. Mar. Biol. Assoc. U.K.*, **57**, 399–354.

Smith, P. C., 1983: The mean and seasonal circulation off southwest Nova Scotia. *J. Phys. Oceanogr.*, **13**, 1034–1054.

——, 1989a: Circulation and dispersion on Browns Bank. *Can. J. Fish. Aquat. Sci.*, **46**, 539–559.

——, 1989b: Seasonal and interannual variability of current, temperature and salinity off southwestern Nova Scotia. *Can. J. Fish. Aquat. Sci.*, **46**(Suppl. 1), 4–20.

Sutcliffe, W.H., Jr., R. H. Loucks, and K. F. Drinkwater, 1976: Coastal circulation and physical oceanography of the Scotia Shelf and the Gulf of Maine. *J. Fish. Res. Board Can.*, **33,** 98–115.

Tee, K. T., 1976: Tide-induced residual current, a 2-D nonlinear numerical tidal model. *J. Mar. Res.*, **34,** 603–628.

——, 1977: Tide-induced residual current—Verification of a numerical model. *J. Phys. Oceanogr.*, **7,** 396–402.

——, 1979: The structure of three-dimensional tide-generating currents. Part I: Oscillating currents. *J. Phys. Oceanogr.*, **9,** 930–944.

——, 1980: The structure of three-dimensional tide-induced current. Part II: Residual current. *J. Phys. Oceanogr.*, **10,** 2035–2057.

——, 1985: Depth-dependent studies of tidally induced residual currents on the sides of Georges Bank. *J. Phys. Oceanogr.*, **15,** 1818–1846.

——, 1987: Simple models to simulate three-dimensional tidal and residual currents. Three-dimensional coastal ocean models. *Coast Estuarine Sci.*, **4,** 125–147.

——, 1993: Dynamics of two-dimensional topographic rectification process. *J. Phys. Oceanogr.*, (in press).

——, and D. Lefaivre, 1990: Three-dimensional modeling of the tidally-induced residual circulation off southwest Nova Scotia. Residual currents and long-term transport. *Coast Estuarine Studies,* **38,** 79–92.

——, P. C. Smith, and D. Lefaivre, 1987: Modelling and observations of the residual current off southwest Nova Scotia. *Proc. Eighteenth Int. Liege Colloq. on Ocean Hydrodynamics,* Elsevier Oceanogr. Ser., **45,** 455–470.

——, P. C. Smith, and D. Lefaivre, 1988: Estimation and Verification of tidally induced residual currents. *J. Phys. Oceanogr.*, **18,** 1415–1434.

Zimmerman, J. T. F., 1986: The tidal whirlpool: A review of horizontal dispersion by tidal and residual currents. *Neth. J. Sea Res.*, **20,** 133–154.